

Design of a mm-wave Planar CPW-fed Tapered Dielectric Rod Antenna

by

Zahra Sotoodeh

A thesis
presented to the University of Waterloo
in fulfillment of the
thesis requirement for the degree of
Master of Applied Science
in
Electrical and Computer Engineering

Waterloo, Ontario, Canada, 2011

© Zahra Sotoodeh 2011

AUTHOR'S DECLARATION

I hereby declare that I am the sole author of this thesis. This is a true copy of the thesis, including any required final revisions, as accepted by my examiners.

I understand that my thesis may be made electronically available to the public.

Abstract

The demand for high data rate transfers in short range areas have been increasing significantly. Millimeter wave communication systems can fulfill the requirements for such applications due to the availability of wide bandwidths at these frequencies. Particularly, 60 GHz frequency band is more appropriate among other mm-wave bands because of the oxygen energy absorption resonance at this frequency.

Millimeter wave antennas are one of the desired components in short range wireless communications. High gain and broadband antennas are required for this purpose.

In this study, a fully planar 60 GHz antenna is introduced. Tapered dielectric rod antenna is chosen to achieve high radiation efficiency. The antenna is designed on two common substrates with high permittivity: alumina (Al_2O_3) and high resistive Silicon. Both substrates are very low loss and many designs for front-end components are developed on these substrates due to their high permittivity. In other words, the proposed antenna can be integrated with the front-end platform in the same substrate. In addition, the antenna feeding is the CPW line which makes it a convenient solution for integration of the antenna with RF front-ends such as MMICs or MEMS circuits in this range of frequency.

Acknowledgements

It is an honor for me to thank those who made this work possible. This thesis would not have been completed without their support and valuable assistance. First and foremost, I would like to express my deepest gratitude to my supervisor, Professor Safavi-Naeini for his continuous and tireless supports and encouragements. I appreciate all your patience and helpful advice during this work.

I would also like to thank Professor Raafat Mansour who kindly accepted to attend my seminar and review my thesis. I also wish to convey thanks to Dr. Simarjeet Saini for reviewing this thesis and providing helpful feedback.

During my study, I have had the opportunity to work with and learn from several brilliant individuals. My special thanks are due to Behzad Biglarbegian, Dr. Mohammad-Reza Nezhad-Ahmadi, and Dr. Mohammad Fakharzadeh for their generous and unselfish sharing experiences and guidance. I am also grateful to thank my colleges Dr. Maher Bakri-Kassem and Saman Jafarloo. The discussions we had during our weekly meetings and the friendly atmosphere they provided, were very helpful for me to know my weaknesses and enhance my research.

I would like to thank Chris Schroeder who kindly edited my thesis. Thanks are also due to Electrical and Computer Engineering (ECE) department staff, especially Susan King, Karen Schooley, Phil Regier, and Fernando Rivero Hernandez, for their cooperative efforts and assistance.

During the study, there are discouraging and hard times for everyone. In such periods, a friendly environment full of love and life would work much better than one's own office. I would like to thank Lynn Rivait, who provides such environment at CEIT café. Thanks for all your positive outlook and caring during the hard times.

I consider myself lucky to have a kind and supportive family. Special thanks are due to my husband, my parents and my parents in law for their nonstop love and support. I would also like to thank My brother, Mostafa, my sister, Mahsa, and my brothers in law, Mohammad and Mehrdad for their encouragements.

This research was supported by National Science and Engineering Research Council (NSERC) of Canada and Research in Motion (RIM).

Dedication

I dedicate this thesis to my family, especially

- to my father, who taught me that the most important thing in one's life is truth and honesty
- to my mother, who taught me how to live every moment with love and hope, no matter how enormous difficulties are
- to my husband, Behzad who radiates immeasurable love to our together life

Table of Contents

AUTHOR'S DECLARATION.....	ii
Abstract.....	iii
Acknowledgements.....	iv
Dedication.....	v
Table of Contents.....	vi
List of Figures.....	viii
Chapter 1 Introduction.....	1
1.1 Objective and Motivation.....	1
1.2 Overview.....	2
Chapter 2 Definition of mm-wave Frequency Band and its Applications.....	3
2.1 Introduction.....	3
2.2 Definition.....	3
2.3 Applications.....	3
2.4 Millimeter Wave Antennas.....	6
2.5 Recent Developments on mm-wave Antennas.....	6
2.6 Summary.....	11
Chapter 3 Wave Propagation in Rectangular Dielectric Waveguides.....	13
3.1 Introduction.....	13
3.2 Dielectric Waveguide Structures.....	13
3.3 Propagation Modes and Field Polarizations.....	13
3.4 DW Dimensions for Operating at 60 GHz Frequency.....	18
3.5 Summary.....	20
Chapter 4 CPW-fed Tapered Dielectric Rod Antenna on Alumina Substrate.....	21
4.1 Introduction.....	21
4.2 Dielectric Rod Antennas.....	21
4.3 Antenna Design.....	22
4.4 Excitation Method for Tapered DW Antenna.....	25
4.5 CPW to Slot Line Transition Design.....	27
4.5.1 Literature Review on CPW to Slot Line Transitions.....	28
4.5.2 CPW to Slot Line Transition Design.....	30
4.6 Single Element CPW-fed Tapered DW Antenna.....	32

4.7 Curved Tapering of Dielectric Rod Antenna.....	34
4.8 Linear Array of Two Elements Antenna	36
4.9 Fabrication Process.....	38
4.10 Summary	39
Chapter 5 Antenna Design on High Resistive Silicon Substrate	40
5.1 Introduction	40
5.2 Mechanical Support Requirement	40
5.3 Design of the CPW to Slot Line Transition on High Resistive Silicon.....	40
5.4 Single Element Tapered Dielectric Antenna on High Resistive Silicon	42
Chapter 6 Conclusion and Future Work.....	45
6.1 Conclusion.....	45
6.2 Future Work	45
Bibliography	46

List of Figures

Figure 2-1 Definition of mm-wave frequencies and their applications (Figure 1.1 from reference [2])	4
Figure 2-2 Unlicensed 60 GHz frequency band allocations in different countries (Figure 5.3 from reference [1]).....	4
Figure 2-3 Oxygen absorption of energy in terms of frequency (Figure 1.1 from reference [1]).....	5
Figure 2-4 Examples of proposed patch antenna designs at 60 GHz: (a) 2×2 array (Fig. 4 of reference [7]), (b) 8×8 array (Fig.2 of reference [9]), and (c) stacked patch (Fig. 2 of reference [8])	7
Figure 2-5 Proposed Yagi-Uda antenna in [12] (Fig. 1 of reference [12])	8
Figure 2-6 Ring slot excited dielectric rod antenna proposed in [13] (Figure 1 of reference [13])	9
Figure 2-7 Image NRD guide dielectric rod antenna proposed in [14] (Fig.1 of reference [14]).....	10
Figure 2-8 Dielectric rod antenna proposed in [15] (Fig. 1 and Fig. 4 of reference [15])	10
Figure 2-9 Integrated front-end at 60 GHz proposed in [16] (Fig. 1 of reference [16])	11
Figure 3-1 Geometry of DW problem in general form.....	14
Figure 3-2 Problem geometry assumed in Marcatili method.....	14
Figure 3-3 Field pattern of first four modes in a rectangular DW (Fig. 5 of reference [20]).....	15
Figure 3-4 Propagation plot for different modes of a rectangular dielectric waveguide (Fig. 6 of reference [20]).....	16
Figure 3-5 Propagation curves of the first two modes in a rectangular dielectric waveguide for various Δn (Fig. 21 of reference [18])	17
Figure 3-6 Propagation curve of the first mode for various aspect ratios (Fig. 22 of reference [18]) .	17
Figure 3-7 Propagation curves ($\mathcal{P}2$) versus frequency for various aspect ratios (substrate is alumina with thickness of 10 mil).....	18
Figure 3-8 (a) DW configuration, and (b) its electric field polarization for the fundamental mode....	19
Figure 3-9 Simulated S parameters result for the DW with aspect ratio of 9	19
Figure 4-1 Various methods of tapering for dielectric rod antenna (Table I of reference [27])	22
Figure 4-2 Dielectric rod antenna configuration: (a) 3-D view, (b) top view	23
Figure 4-3 Simulated maximum Gain versus length of the antenna	23
Figure 4-4 Simulation result for E-plane and H-plane pattern of the DW antenna.....	24
Figure 4-5 Simulated return loss of the DW antenna.....	24
Figure 4-6 Simulated Gain versus frequency for the DW antenna	25
Figure 4-7 DW antenna with slot-line excitation and its corresponding gain pattern.....	26

Figure 4-8 Simulation results for DW antenna with slot line excitation: (a) Gain pattern, and (b): S_{11}	27
Figure 4-9 CPW-to-Slot line transition configurations: (a) Figure 1 of reference [38], (b) Fig. 1 of reference [32], (c) Fig. 3 and Fig. 9 of reference [34], (d) Fig. 3 of reference [35], and (e) Fig. 1 of reference [36]	29
Figure 4-10 CPW-to-Slot line transition for 60 GHz operational frequency	30
Figure 4-11 Field distribution at the x direction over different cross sections of the transition.....	31
Figure 4-12 Simulated S parameters result of the CPW-to-Slot line transition	32
Figure 4-13 Single element antenna configuration.....	33
Figure 4-14 E-plane and H-plane gain pattern of the single element antenna.....	33
Figure 4-15 Simulated return loss plot for single element antenna	34
Figure 4-16 Single element antenna with exponential tapering	35
Figure 4-17 Simulation result of gain for the antenna with exponential tapering	35
Figure 4-18 Return loss simulation result for antenna with exponential tapering.....	36
Figure 4-19 Linear array of two elements antenna configuration	37
Figure 4-20 Simulation result of the gain pattern for the array antenna.....	37
Figure 4-21 Simulation result of the return loss for the array antenna	38
Figure 5-1 CPW to slot line transition on high resistive silicon substrate.....	41
Figure 5-2 Layer configuration of the CPW to slot line transition.....	41
Figure 5-3 Simulation results of S parameters for the CPW to slot line transition on HR silicon	42
Figure 5-4 Single element antenna on high-resistive silicon: (a) 3D view, and (b) bottom view	43
Figure 5-5 Simulation result of gain for the single element antenna on high- resistive silicon	44
Figure 5-6 Return loss simulation result for single element antenna on high-resistive silicon	44

Chapter 1

Introduction

1.1 Objective and Motivation

The development of high definition audio/video signals and the growing number of communicating devices in homes have recently brought the demand for high data rate wireless communication in short ranges. The mm-wave frequencies are one of the best candidates for this goal. The mm-wave frequency bands offer a wide bandwidth, allowing the communication data rates up to 5 Gbits/sec. In addition, from commercial point of view, fabrication techniques have been recently developed to provide high efficiency and low cost circuits in this range of frequency. However, due to the free space loss of the signal in the mm-wave band, the applications are limited to short ranges such as WPAN¹.

Among various mm-wave frequency bands, 60 GHz frequency band has special properties, making it more appropriate for wireless communications in short ranges. In North America, a 7 GHz free licensed bandwidth has been allocated for researchers in this area. The frequency band is in the range of 57 GHz to 64 GHz [1]. More details on 60 GHz characteristics and mm-wave applications are given in Chapter 2.

When designing a wireless communication link, antenna is one of the critical building blocks. In 60 GHz short range applications, high gain (more than 10 dB) and broadband antennas are desired. In order to have a complete communication link, the antenna is integrated with other active and passive components such as amplifiers, filters, and phase shifters. Therefore, besides the antenna gain and bandwidth, many parameters come to the picture such as cost, size, realization complexity, and more importantly, compatibility with active and passive circuits and components. Considering these parameters, a planar antenna is preferred. In addition, having the antenna and other components on the same substrate, facilitate the integrity of the entire system.

Based on the aforementioned issues, the objective of this research is to introduce a planar CPW-fed high gain and broadband antenna design for 60 GHz short range applications. The antenna design on two different substrates is explained in this report. The planar antenna with CPW feed can be easily connected to 60 GHz front-end components and circuits. In addition, the CPW line allows exploiting the flip-chip technique to assemble active MMIC devices prior to the antenna. The two substrates

¹ Wireless Personal Area Network

used in this report are alumina and high resistive silicon. Both materials have high permittivity and very low loss, resulting in high efficient and low profile integrated systems. Both substrates are common in designing various types of mm-wave circuits. Therefore, having the antenna design on these substrates would smooth the integration process for a monolithic and compact communication link.

1.2 Overview

The mm-wave frequency band definitions and its applications are briefly described in Chapter 2. The chapter is followed by a literature review of recent works on mm-wave antennas. Tapered dielectric rod antennas are proposed as a good candidate for short range applications.

Dielectric waveguides are the building blocks of the tapered dielectric rod antennas. The wave propagation in rectangular dielectric waveguides is studied in Chapter 3. The propagation mechanism in dielectric waveguides is briefly explained and the existing numerical solution methods are summarized. Consequently, the propagation modes, the fundamental mode pattern, and the remarkable affecting factors on the dielectric waveguide characteristic are given in this chapter. Finally, the explained methods are applied to specify the required dielectric waveguide dimensions for this project, knowing the operating frequency range and the dielectric material.

A CPW-fed tapered dielectric rod antenna design is explained in Chapter 4. The details of design steps are given and the simulation results are reported in this chapter. Alumina substrate is used in the antenna design. The chapter ends with a discussion on fabrication techniques and existing challenges for the proposed configuration.

The antenna design on high resistive silicon is presented in Chapter 5. The new proposed antenna in this chapter is mechanically stronger structure. In addition, because of silicon properties, etching can be exploited to fabricate the structure. Therefore, the antenna design proposed in this chapter is more realizable from practical point of view.

Finally, conclusion and suggestions for future works are presented in Chapter 6.

Chapter 2

Definition of mm-wave Frequency Band and its Applications

2.1 Introduction

The mm-wave frequency range definition is explained in section 2.2 followed by brief description of its applications in section 2.3. Based on the focus of this study, mm-wave antennas requirements for short range applications are explained in section 2.4. Some examples of recent developments on mm-wave antennas are reported in section 2.5. Finally, the chapter concludes with a summary in section 2.6.

2.2 Definition

The term mm-wave is used for a wide range of frequencies between 30 GHz and 300 GHz. It is called mm-wave because the wavelength is varying from 1 to 10 millimeters for this range of frequency.

2.3 Applications

There are many applications for mm-waves varying from radar and communications to disease diagnosis and imaging. Wireless short range communications, radar sensors, point-to-point access for backhaul applications, and imaging are some of the examples of mm-wave applications [2]. Available mm-wave bands and their corresponding applications are summarized in Figure 2-1. The interest of this study is the application of mm-wave in wireless short range communications.

In short range wireless communications, utilizing mm-waves can facilitate high data rate transfers. Transferring uncompressed audio and video signals from laptop to LCD, picture downloading from camera/cell phone to laptops and wireless video projecting from laptop to the screen are some examples of this application [3]. This class of short range wireless communication is known as Wireless Personal Area Network (WPAN).

Millimeter wave front-ends have recently attracted considerable attention since the need for high speed data rates is growing significantly. As mentioned before, there are number of allocated unlicensed/easily licensed frequency bands available for researchers in this area (see Figure 2-1). 60 GHz band is particularly of interest among these bands for some reasons. The most important reason is its overlap with the oxygen absorption resonance range. The oxygen energy absorption versus frequency curve is plotted in Figure 2-3. As can be observed from this plot, more than 98% of energy

absorbs at a distance of 1 km at this frequency. Due to the huge amount of absorption, as well as the free space attenuation, 60 GHz band cannot be used for long distance wireless communications. However, the oxygen absorption is considered as a good feature in short ranges since it allows the frequency reuse within near cells. In other words, the high absorption provides interference free regions with close distances to each other. Because of the efficiency improvement in this particular band (60 GHz), it is considered more suitable for short range applications rather than other mm-wave frequency bands. The details on the allocated 60 GHz frequency band in different countries are given in Figure 2-2.

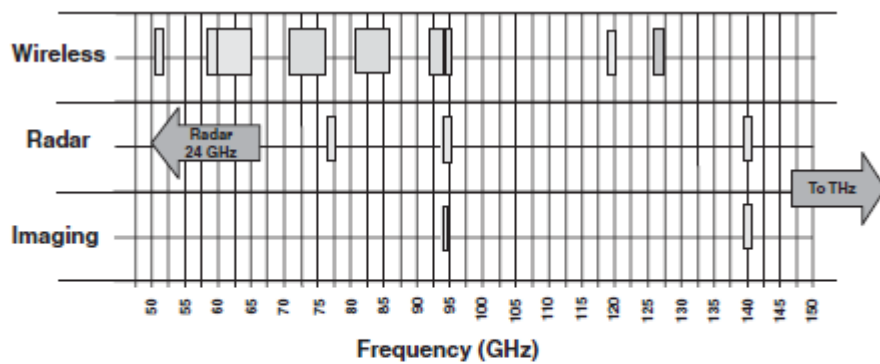


Figure 2-1 Definition of mm-wave frequencies and their applications (Figure 1.1 from reference [2])

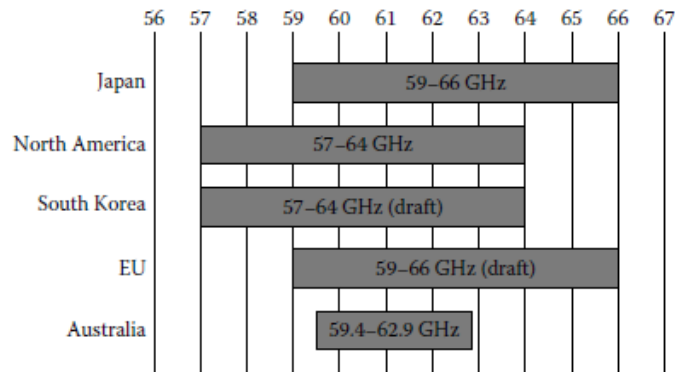


Figure 2-2 Unlicensed 60 GHz frequency band allocations in different countries (Figure 5.3 from reference [1])

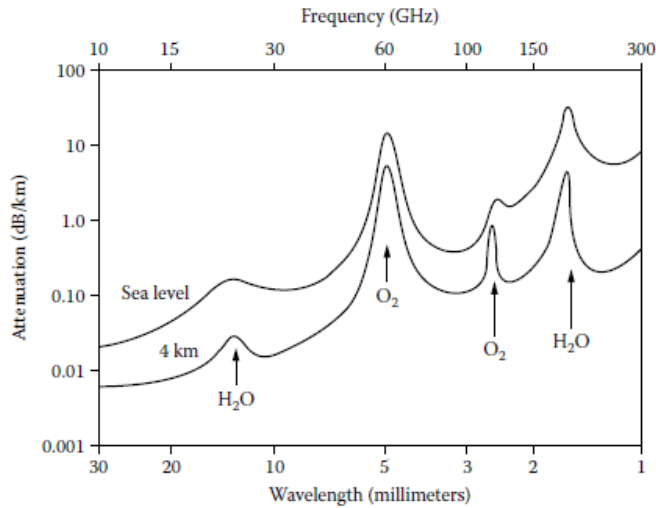


Figure 2-3 Oxygen absorption of energy in terms of frequency (Figure 1.1 from reference [1])

Based on the aforementioned applications, different standards have been developed as a guide for designing wireless communication links at 60 GHz frequency. There are three groups working on standardization of 60 GHz wireless communication [1]: IEEE802.15.3c working group [4], WirelessHD [5], and the WIGWAM project [6].

IEEE802.15.3c group has developed standards for high data rate wireless communications at 60 GHz. In the IEEE standard, different wireless connectivity applications are categorized to three classes: Class 1 is used for ‘low-power low-cost mobile market’ with data rates lower than 1.5 Gb/s. Class 2 belongs to data rates up to 3 Gb/s, and class 3 is specified for ‘high performance applications’ with data rates above 3 Gb/s. The requirements for each class have been defined and can be accessed in [4].

The WirelessHD group’s interest [5] is mostly the high speed A/V streaming for consumer electronic devices [1]. The group target is using low power amplifiers combined with high gain antennas.

WIGWAM (Wireless Gigabit With Advanced Multimedia Support) consist of many European research groups and their target is wireless communication systems with data rates of maximum 1 Gb/s. They have chosen the 5 GHz band as preliminary implementation while looking at extension bands of 17, 24, and 60 GHz. The updated information can be accessed through [6].

2.4 Millimeter Wave Antennas

Antenna is one of the most important building blocks in designing 60 GHz communication links. There are many issues that need to be taken into account when designing an antenna in mm-wave frequencies. For any application, common antenna parameters such as gain, bandwidth, and efficiency need to meet certain specifications. In addition to those requirements, many fabrication and price issues come to the picture when designing the antenna at mm-wave frequencies. The capability of the antenna to be integrated with other components of a complete front-end is another aspect in mass production level.

In many applications of 60 GHz short range and high speed wireless communications, high gain (more than 10 dB) antennas are required [7]. The bandwidth of such antennas should preferably cover the entire frequency band, i.e. 57 GHz to 64 GHz. This leads to an approximately 11.5% bandwidth. Therefore, a relatively high gain and broadband antenna is desired.

2.5 Recent Developments on mm-wave Antennas

A variety of antenna structures have been proposed for operating in mm-wave frequencies. They can be classified in two categories: conductor-based antennas and dielectric-based antennas.

In the conductor-based antennas, the electromagnetic energy is being transmitted through the conductors. In other words, the source of radiation in this class of antennas is typically the electric current. The common examples of this category are patch and Yagi antennas ([8], [9], [10], [7], [11] [12]). In the conductors, the surface impedance is proportional to the operating frequency. The relationship between the surface impedance of a conductor and frequency is:

$$(1) \quad R_s = \frac{1}{\sigma\delta} = \sqrt{\frac{\omega\mu}{2\sigma}}$$

Where δ and σ are the skin depth and the conductivity of the conductor respectively. As can be seen from this equation, the surface impedance is increased with increment of operating frequency. As a result, the conductor loss increases significantly at high frequencies. Therefore, the conductor-based antennas present lower efficiency at higher frequencies. Some of the examples of this class of antennas designed to operate at 60 GHz band are explained as follow:

Patch antennas have attracted extensive attention because of their planar structure, small size, and simple configuration. However, they are not essentially high gain elements [10]. In order to obtain

relatively high gains, arrays of patch antennas should be constructed. A 2×2 planar arrays of patch antenna have been proposed in [7] to operate at 60 GHz frequency. Figure 2-4(a) shows the proposed array structure. The antenna gain of more than 10 dB has been achieved for this structure. The 10 dB bandwidth of the configuration is reported to be about 7% and the antenna efficiency has not been reported. Another planar array configuration is proposed in [9] and the configuration is depicted in Figure 2-4 (b). The measurement has been done for a 4×4 array and then, the characteristic parameters of the 8×8 array are calculated based on the results of the 4×4 array. For the 4×4 array, the gain has been reported to be 14.1 dB as measured at 59.5 GHz. However, the reported frequency bandwidth is 3.4 % and the efficiency is reported to be 43%. The low efficiency is basically because of conductor loss in feeding network, which is increased drastically by increasing the number of elements. Therefore, the high gain has been achieved at the cost of efficiency.

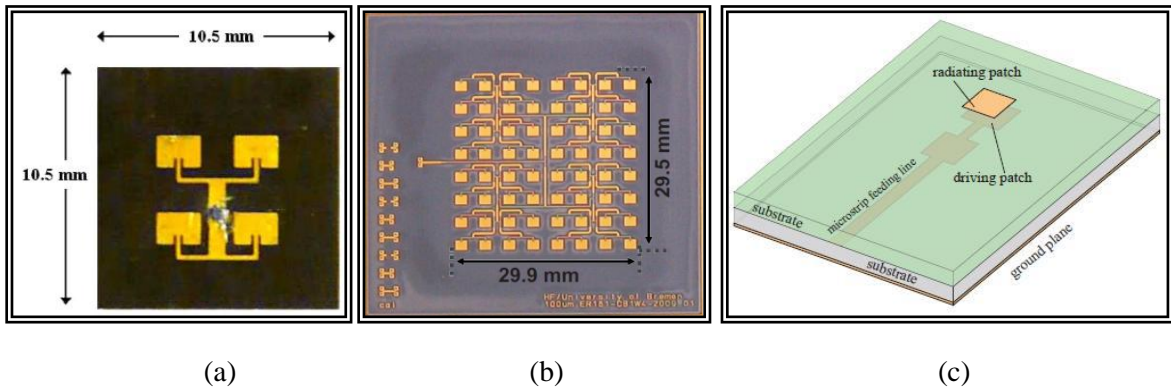


Figure 2-4 Examples of proposed patch antenna designs at 60 GHz: (a) 2×2 array (Fig. 4 of reference [7]), (b) 8×8 array (Fig.2 of reference [9]), and (c) stacked patch (Fig. 2 of reference [8])

In [8], a stacked patch antenna has been introduced (see Figure 2-4(c)). Two driving patches are connected in series in this structure to feed the radiating patch in upper layer. The first driving patch is radiating as well, constructing array of two elements in different layers. The second series patch is acting as a load for the first patch, while driving the upper radiating patch simultaneously. The reported results for this antenna shows a significant enhancement in frequency bandwidth (the impedance bandwidth has been reported to be 22% approximately) while having more than 8 dB gain at the entire frequency range. The antenna efficiency has not been reported in this paper.

Yagi-Uda is another conventional configuration in planar conductor-based class of antennas. An antenna of this type has been proposed in [12] for operating at 60 GHz frequency band. The proposed configuration is illustrated in Figure 2-5.

The corrugated ground plane in this structure acts as the reflector for Yagi-Uda antenna. The reported results show a frequency bandwidth of about 8 % with more than 9 dB gain on the entire bandwidth. The efficiency is reported to be 95%. However, the feeding loss has not been included in efficiency calculations.

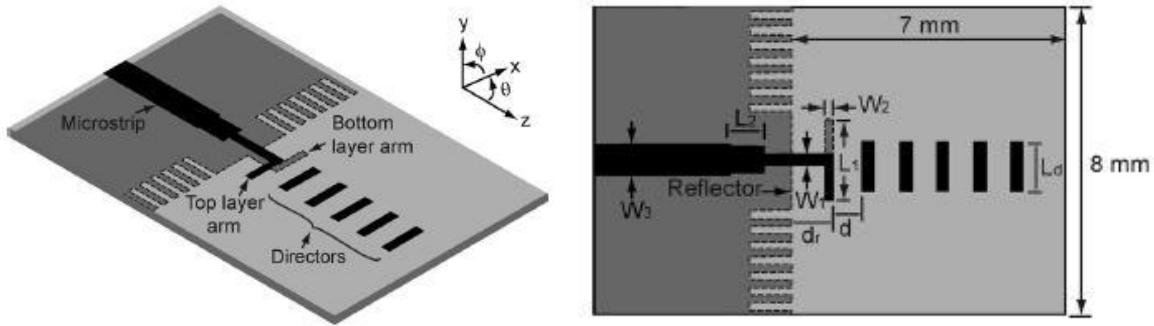


Figure 2-5 Proposed Yagi-Uda antenna in [12] (Fig. 1 of reference [12])

As mentioned before, most of the conductor-based antenna designs suffer from lower efficiency at mm-wave frequencies. In addition, all the structures explained above are developed on substrates with relatively low dielectric constants ($\epsilon_r = 2\sim 3$). In the substrates with higher permittivity, the quality factor of the antenna increases since more electromagnetic energy can be stored. Therefore, the operation bandwidth, which is inversely proportional to the quality factor, is decreased. On the other hand, dielectric materials with relatively high permittivity ($\epsilon_r > 9$) are desirable for designing the RF front-ends of a communication link. In these substrates, the guided wavelength decreases and as a result, the components which use transmission lines become smaller. This leads to realize miniaturized integrated communication systems. Hence, having an antenna design on substrate with high permittivity leads to a monolithic system and the entire communication link can be fabricated over one process.

Considering those issues, dielectric-based antennas come to the picture as good candidates in mm-wave frequencies. The radiation source in this class of antennas is leaking waves or surface waves transferring through the dielectric materials. Unlike the conductor-based antennas, dielectric-based antennas are typically fabricated on very low loss materials with high permittivity. As a result, this class of antennas exhibit very high efficiencies at mm-wave frequencies. Some of the proposed dielectric antennas for mm-wave applications are summarized below:

A dielectric rod antenna with ring slot excitation is introduced in [13]. The antenna is operating at 550-650 GHz frequency band (16% bandwidth). The geometry of this antenna is depicted in Figure 2-6. A ring slot in a ground plane has been attached to the antenna in order to excite the dielectric rod. The cross section of the dielectric rod is tapered gradually as illustrated in Figure 2-6. A gain of 10 dB has been reported for this configuration and the reported efficiency is 90% at the centre frequency.

A linear array of image NRD guide² dielectric rod antennas is proposed in [14]. The structure is illustrated in Figure 2-7. Each antenna element consists of a tapered dielectric rod antenna which is connected to an image NRD guide. A transition has been designed from dielectric rod antenna to image NRD guide. As can be seen in Figure 2-7, the image NRD guides in the linear array are excited by coupling from rectangular slot in a common waveguide along the array. The operating frequency for this configuration is 35.5 GHz. A very high gain of 22 dB has been reported for the two element array. The length of dielectric rods is equal to $10.6 \lambda_0$, which is 90 mm at 35 GHz frequency. The frequency bandwidth for this structure is about 1.5 %.

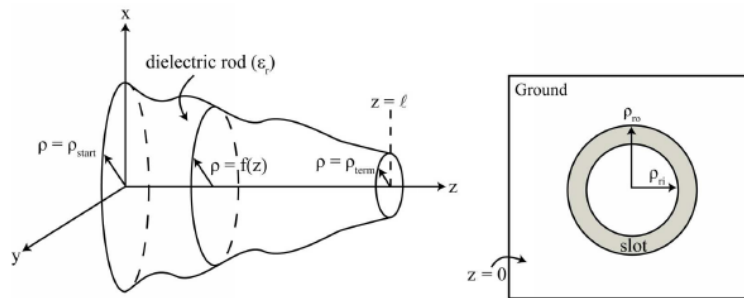


Figure 2-6 Ring slot excited dielectric rod antenna proposed in [13] (Figure 1 of reference [13])

² NonRadiative Dielectric guide

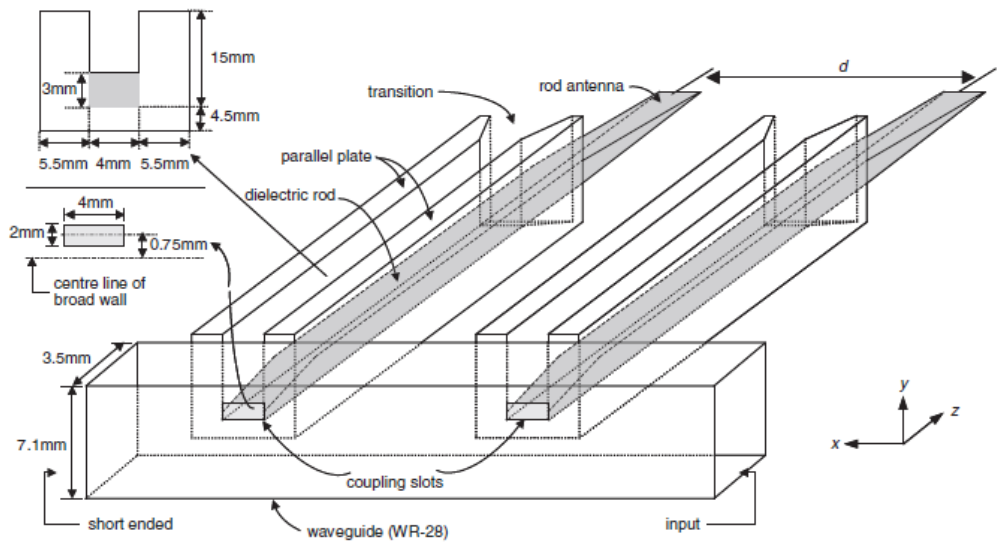


Figure 2-7 Image NRD guide dielectric rod antenna proposed in [14] (Fig.1 of reference [14])

Another configuration for dielectric rod antenna is proposed in [15]. In this design, substrate integrated image guide (SIIG) is employed to excite the tapered dielectric rod antenna (see Figure 2-8). The SIIG has been realized by perforating the dielectric on both sides of the desired width. The air holes result in reduction of effective dielectric constant in those areas, leaving the desired image guide in between. A transition from metallic waveguide to the SIIG has been design at the input port. A half pyramidal horn has been formed in an aluminum block for this approach. The antenna is working at 94 GHz frequency. The achieved gain is 12.8 dB and the frequency bandwidth is approximately 8 %.

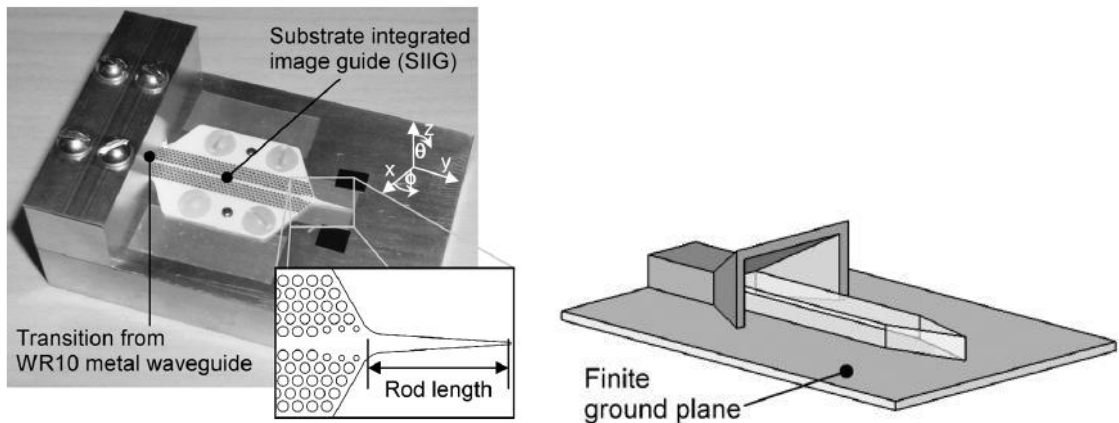


Figure 2-8 Dielectric rod antenna proposed in [15] (Fig. 1 and Fig. 4 of reference [15])

The aforementioned antennas are fabricated on low loss materials with high permittivity. From integration point of view, [14] is a 3D structure and cannot be used in a planar system. Although the introduced design in [15] shows a planar structure, the excitation section which is a semi-horn configuration is not compatible with common planar waveguides such as CPW. Scaling the proposed design in [13] for 60 GHz frequency leads to mechanically unstable structure because the standing dielectric rods will be much longer at 60 GHz.

In [16], an active front-end with integrated dielectric antenna is introduced. The proposed configuration is presented in Figure 2-9. The CPW line is chosen as the input of this front-end. For the CPW to SIIG transition, the proposed configuration in [17] has been exploited. The simulated antenna gain is 11.5 dB and the radiation efficiency is reported to be more than 80% in this design. The antenna beam is tilted from the end-fire direction because of the presence of the ground plane in this design. In addition, a planar structure without ground plane is preferred to prevent any back metallization process.

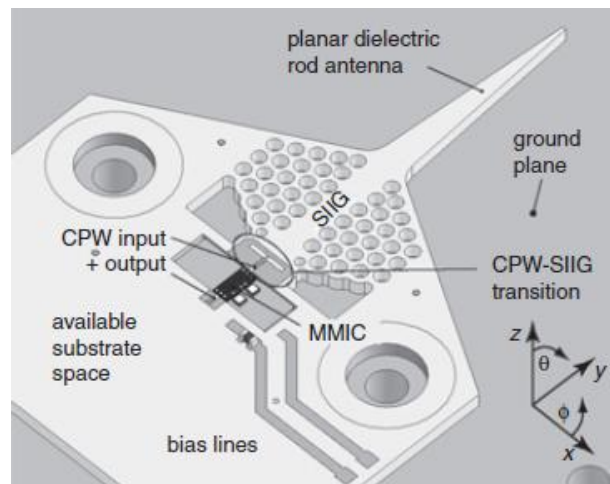


Figure 2-9 Integrated front-end at 60 GHz proposed in [16] (Fig. 1 of reference [16])

2.6 Summary

High gain and wide band antennas are required for various mm-wave applications. Planar geometries are preferred for antenna structures because of their ease of fabrication and integration. On the other hand, antennas on low loss and high permittivity materials are interested since they are compatible with front-end mm-wave circuits and modules, facilitating the realization of monolithic integrated communication links. Various planar structures have been proposed ([10]-[12]) but most of

them are conductor-based and also fabricated on substrates with low dielectric constants. A low dielectric constant improves the antenna bandwidth of this class. However, it is less compatible with mm-wave components which are fabricated on high permittivity materials, taking the advantage of miniaturized sizes. In addition, they have lower radiation efficiency due to the significant increase in conductor loss at mm-wave frequency bands.

Unlike the conductor-based antennas, dielectric rod antennas are typically fabricated on very low loss materials with high dielectric constants. However, most of the proposed structures are not fully planar ([13]-[15]), a disadvantage when seeking for a low profile integrated system.

Chapter 3

Wave Propagation in Rectangular Dielectric Waveguides

3.1 Introduction

Rectangular dielectric waveguides are studied in this chapter. The need for dielectric waveguides at high frequencies is enlightened in section 3.2, including a brief explanation on the fundamental differences between dielectric and metallic waveguides characteristics. Propagation modes and corresponding field polarizations in dielectric waveguides are presented in section 3.3. Dielectric waveguide dimensions are determined in section 3.4 for operation at 60 GHz frequency. Last section, section 3.5, contains a summary of the contents of this chapter.

3.2 Dielectric Waveguide Structures

In order to fulfill the rapidly growing demand for broadband and high data rates in wireless communications, the operating frequency needs to be increased. At such high frequencies, the conductor loss is increased significantly due to the increment of surface resistance, reducing the system performance. Therefore, metallic structures are not preferred higher frequencies. Dielectric structures made from very low loss materials are one of the best substitutes at such frequencies. In planar configurations, rectangular dielectric waveguides are the building blocks of any dielectric-based structure.

Rectangular dielectric waveguides have been known for many years. In comparison to their metallic counterparts, they exhibit better performance when operating at mm-wave frequencies. However, unlike the metallic waveguides, the solution of Maxwell equations for rectangular DW³s is very complicated due to the boundary conditions. In other words, no analytical solution exists. Several approximations and numerical methods have been developed to characterize the DWs ([18]-[19]-[20]). The solution for a rectangular DW is explained based on these methods and propagation modes are determined in the following section.

3.3 Propagation Modes and Field Polarizations

The geometry of a rectangular DW problem in general form is illustrated in Figure 3-1. The entire space is divided to nine regions which can be made from different materials in general. The symbol n_i

³ Dielectric Waveguide

in each region represent the refractive index of that region. As mentioned before, the analytical analysis cannot be done for this problem unless using some approximations.

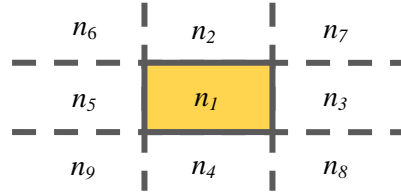


Figure 3-1 Geometry of DW problem in general form

Marcatili [20] has presented an approximate closed form solution for this problem by assuming very weak field intensity in corner regions. In his method, a novel idea is employed to solve the problem. To illustrate the idea, consider the geometry of two dielectric waveguides shown in Figure 3-2. Solution of the original DW problem can be regarded as the asymptotic solution of this new geometry when $c \rightarrow \infty$. As can be seen in Figure 3-2, the geometry is symmetrical about $x=0$ plane. Therefore, only symmetric/anti-symmetric fields exist, resulting in magnetic/electric short circuits at $x=0$.

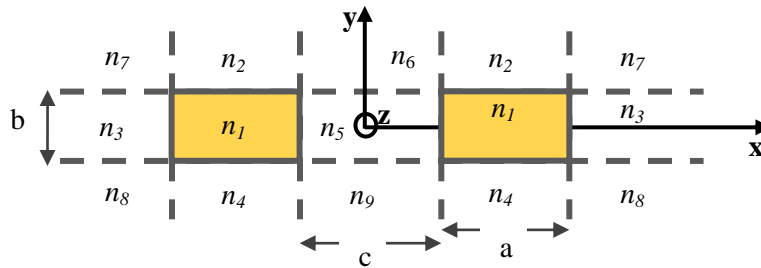


Figure 3-2 Problem geometry assumed in Marcatili method

Considering the geometry shown in Figure 3-2, Marcatili has assumed zero field intensity in regions 6 through 9. Therefore, the boundary condition should be satisfied only on the four side walls of the DW. The other assumption in his method is that the refractive index difference between the DW core and outer areas is very small (less than 1.5). Based on these assumptions, Marcatili has computed two sets of solutions (modes) called E_{mn}^y and E_{pq}^x . The superscript x/y reveals that the most significant component of that field is in x(y) direction. The subscripts mn(pq) indicate the number of maxima and minima in x and y directions respectively. He demonstrated that the two sets of modes are degenerate and the fundamental mode is $E_{11}^x(E_{11}^y)$. Some of the E_{mn}^x mode patterns and their corresponding field polarizations are illustrated in Figure 3-3. The mode patterns of E_{mn}^y can be easily

obtained by interchanging the magnetic and electric fields. In this figure, it is assumed to have $n_3=n_5$ and $n_2=n_4$, leading to symmetric patterns about $x=0$ and $y=0$.

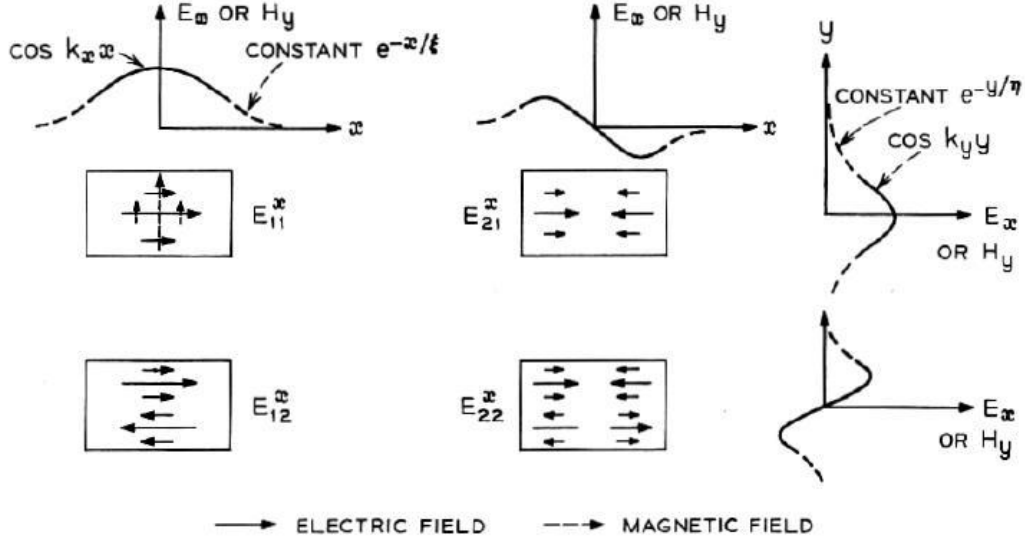


Figure 3-3 Field pattern of first four modes in a rectangular DW (Fig. 5 of reference [20])

To plot the propagation constant curves for different configurations, the DW dimensions and propagation constant (k_z) have been normalized in [20] so that the plots become independent of operating frequency. The normalized propagation constant, \mathcal{P}^2 , is defined as:

$$(2) \quad \mathcal{P}^2 = \frac{k_z^2 - k_4^2}{k_1^2 - k_4^2}$$

This parameter has been plotted versus the normalized waveguide dimension, \mathfrak{B} , which is defined as:

$$(3) \quad \mathfrak{B} = \frac{2b}{\lambda} (n_1^2 - n_4^2)^{1/2}$$

In above formulas, the k_i is the propagation constant corresponding to a free space medium with refractive index of n_i . The normalized propagation constant (\mathcal{P}^2) varies between 0 and 1. The values close to zero indicate weak guidance of the specified mode. On the other hand, the more the value is, the better confinement exists in the DW core, resulting in better guiding. Figure 3-4 shows the propagation curve when the DW is immersed in a medium with refractive index of n_4 . The degeneracy of two sets of modes is apparent in this plot. It is noticeable that the degeneracy does not

depend on the aspect ratio of the DW cross section. The dashed curves are the results of a computational method presented by Goel [18] and are plotted to verify the validity of Marcattily's solution. As can be seen in this figure, the most discrepancy occurs near the cut off region.

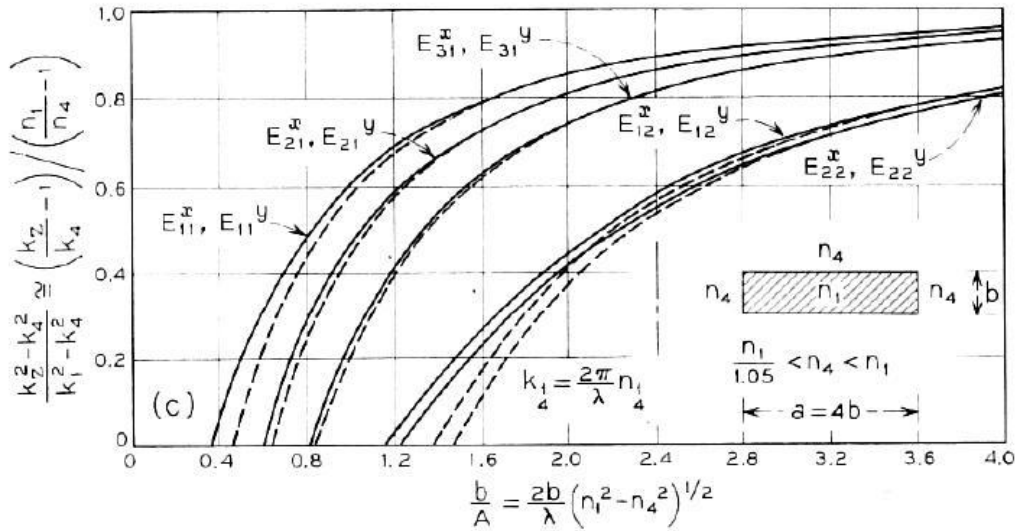


Figure 3-4 Propagation plot for different modes of a rectangular dielectric waveguide (Fig. 6 of reference [20])

Although the approximations presented by Marcattily show an excellent match with numerical results, they cannot be used for the refractive index differences more than 1.5 [20]. When the refractive index difference is increased, the modes are no more degenerate. The fundamental mode is E_{11}^x in this case [18]. Extensive numerical research has been done by Goel to demonstrate this concept [18]. In addition, he has shown that for a certain value of b (the DW height), the cut off frequency of the first mode (E_{11}^x) will increase by increasing the aspect ratio of the DW cross section. The dependency of the propagation curves to the refractive index difference and the aspect ratio are depicted in Figure 3-5 and Figure 3-6 respectively.

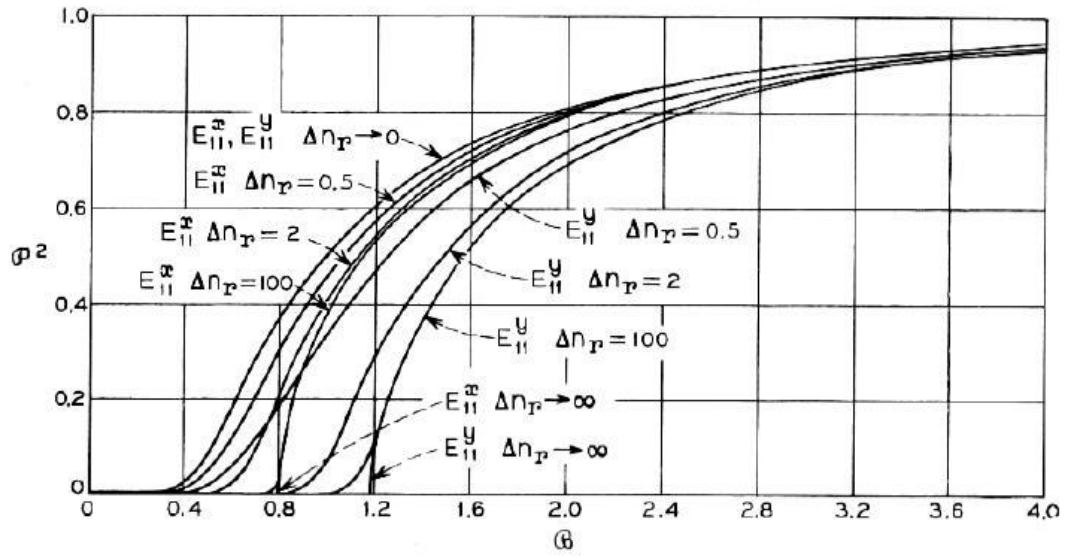


Figure 3-5 Propagation curves of the first two modes in a rectangular dielectric waveguide for various Δn (Fig. 21 of reference [18])

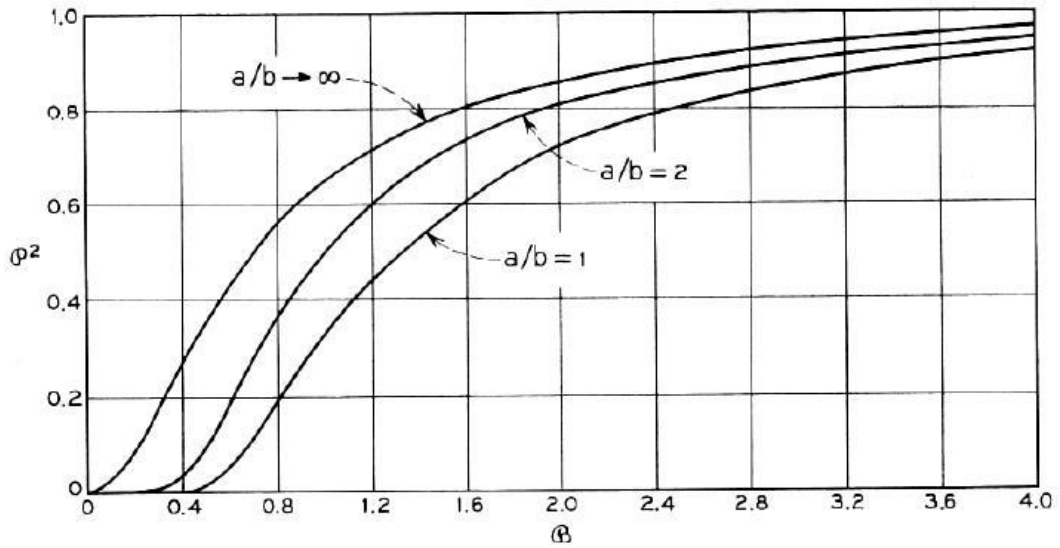


Figure 3-6 Propagation curve of the first mode for various aspect ratios (Fig. 22 of reference [18])

3.4 DW Dimensions for Operating at 60 GHz Frequency

As mentioned in section 1.1, the objective of this thesis is to design a planar DW antenna on two common low loss materials. Alumina and high-resistive silicon are the materials used in this project. The dielectric constant is 9.8 and 11.9 for alumina and silicon respectively. Both substrates are very low loss materials. The substrate is commonly available in different thicknesses from 10 mils to 40 mils. Thicker substrates have more mechanical stability while formation of unwanted substrate modes is prevented by choosing thin substrates [21]. The effective thickness of a substrate is inversely proportional to the guided wavelength in the material and therefore, the choice of substrate thickness is limited as the operating frequency is increased.

In this project, the substrate thickness has been chosen to be 10 mils. The normalized propagation constant (\mathcal{P}^2) versus frequency is plotted in Figure 3-7 for different values of aspect ratio (a/b). As can be seen in this figure, for operating frequency range of 57-64 GHz, the aspect ratios of more than 9 should be selected. The configuration of the DW and its corresponding electric fields pattern is shown in Figure 3-8 when the aspect ratio is equal to 9.

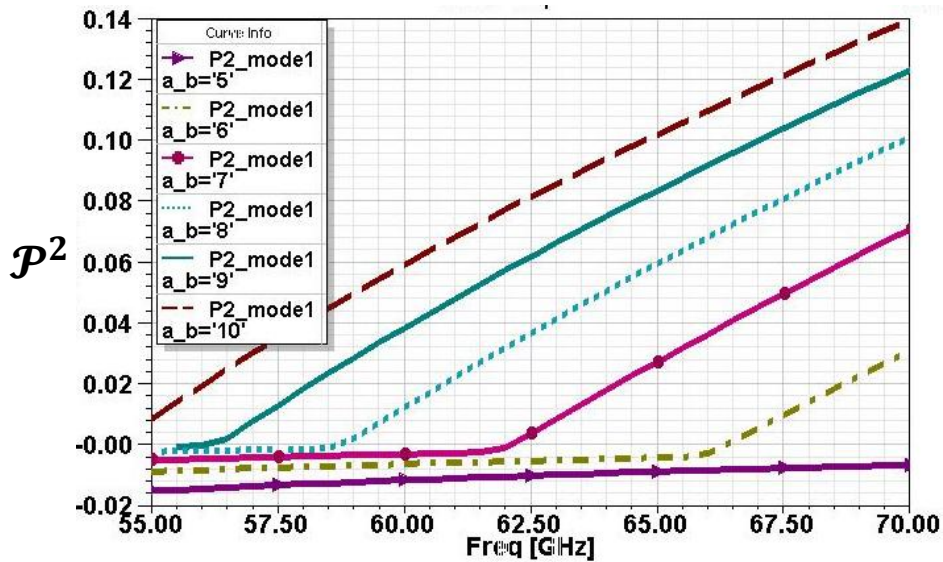


Figure 3-7 Propagation curves (\mathcal{P}^2) versus frequency for various aspect ratios (substrate is alumina with thickness of 10 mil)

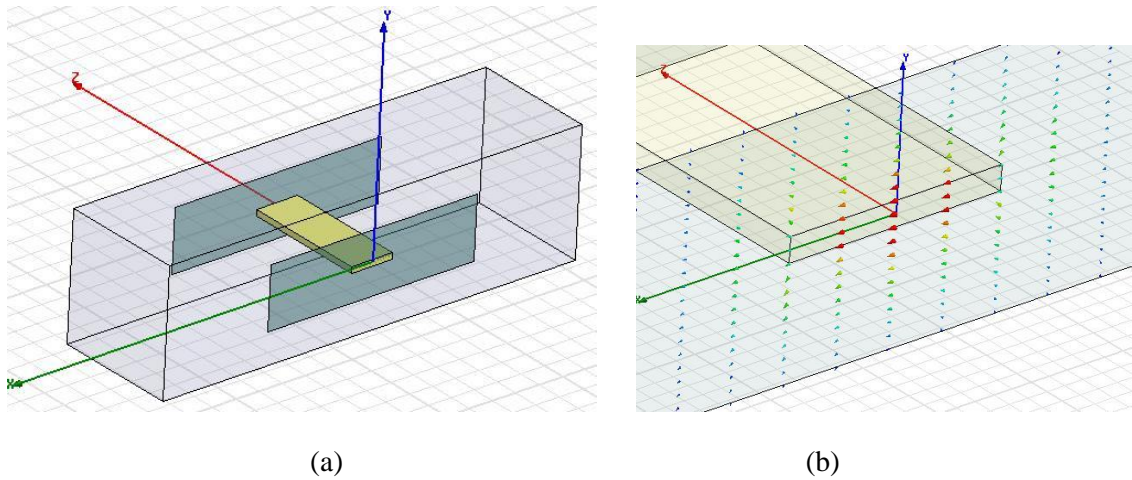


Figure 3-8 (a) DW configuration, and (b) its electric field polarization for the fundamental mode

The structure has been simulated in HFSS and the S parameter results can be observed in Figure 3-9. Propagation starts at 56 GHz frequency as expected from Figure 3-7. The insertion loss is better than 0.5 dB on the desired range of frequency (57-64 GHz).

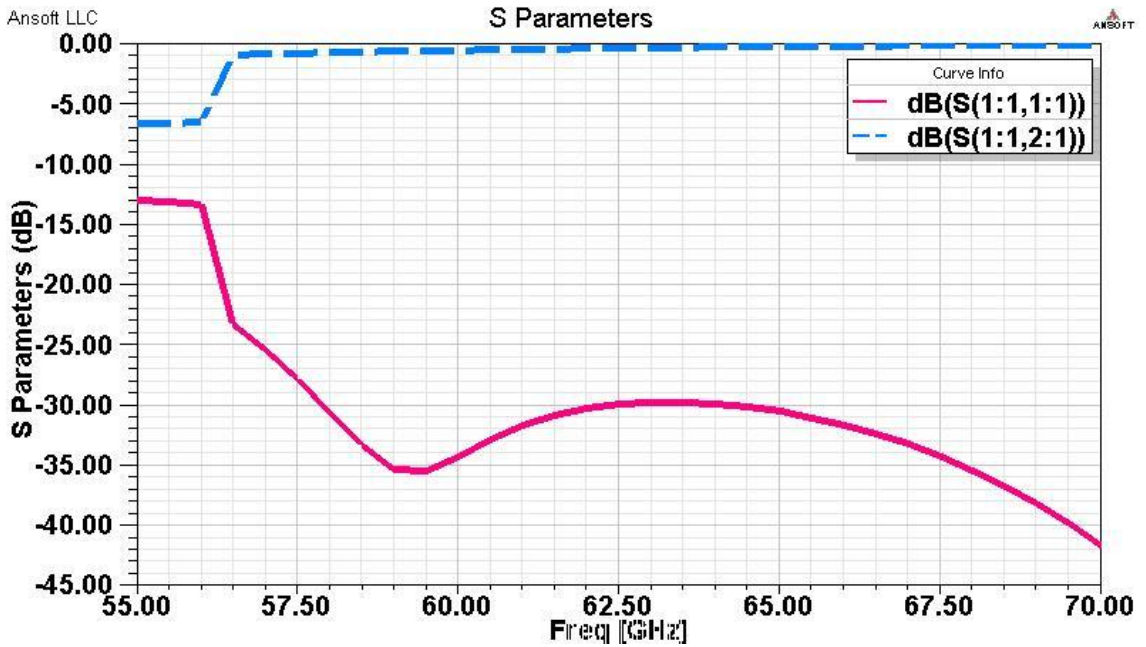


Figure 3-9 Simulated S parameters result for the DW with aspect ratio of 9

3.5 Summary

In this chapter, the behavior of dielectric waveguide structures was studied. The propagation modes were explained and the dimensions for the DW to operating in 57-64 GHz range were determined by assuming a 10 mil alumina substrate. The fundamental mode was shown to be E_{11}^x which means an x-directed electric field with a maximum at centre.

Chapter 4

CPW-fed Tapered Dielectric Rod Antenna on Alumina Substrate

4.1 Introduction

Dielectric rod antenna structures are introduced in section 4.2. Design of a dielectric rod antenna on alumina substrate is presented in section 4.3. The chapter is followed by a discussion on the excitation method for this type of antenna in section 4.4. Based on the conclusion of this section, the details of designing a CPW to slot line transition are given in section 4.5. The simulation results for single element antenna, including its feeding, are presented in section 4.6. Another structure with reduced size is proposed in section 4.7. In order to verify the antenna capability in phased array applications, a two element linear array of the designed antenna is studied in section 4.8. Finally, the fabrication process and summary of the chapter are presented in sections 4.9 and 4.10 respectively.

4.2 Dielectric Rod Antennas

Dielectric tapered antennas have been known for many years. In general, a rectangular dielectric rod is a surface wave structure. If this structure is terminated to free space, the radiation takes place from the dielectric-free space discontinuity ([22], [23]). The radiation performance is improved by slightly tapering the dielectric rod so the traveling wave is transformed to free space radiating wave smoothly. The longer the tapering part is, the more gain the antenna has. Figure 4-1 shows some typical geometry of such antennas.

Although many designs have been reported, there is no exact design procedure for such antennas since theoretical solution is complicated for these antennas [24]. Zucker [25] presented an experimental design method for obtaining maximum gain. In the proposed structure, the antenna is tapered in both directions (E-plane and H-plane) symmetrically. To achieve a simpler structure from fabrication point of view, the effect of tapering in only one direction (E-plane or H-plane) has been investigated by a number of researchers ([14], [26]-[27]). Some examples of different tapered dielectric rod antennas are depicted in Figure 4-1. In [14], it is stated that an E-plane taper would be more mechanically stable. In [27], a complete comparison has been reported between different types of tapering and an optimum shape for the antenna is introduced. With this design, the gain has been improved by one dB at the cost of fabrication complexity. Concluding the results, there is no significant difference between various tapering shapes for this type of antenna [26].






Dielectric rod type	<i>Optimized dielectric rod</i>	<i>Tapered along x</i>	<i>Tapered along y</i>	<i>Tapered at both direction</i>	<i>Circular dielectric rod tapered</i>
The figure of the dielectric rod					

Figure 4-1 Various methods of tapering for dielectric rod antenna (Table I of reference [27])

In this report, the focus is to have a planar structure for the antenna and thus, the antenna is tapered only at the x direction (E-plane tapering).

4.3 Antenna Design

In section 3.4 of this report, the DW dimensions were determined for operation at desired frequency band (57-65 GHz). Recalling from section 3.4, alumina material has been chosen as the design substrate. The loss tangent of alumina is 0.0001 and the relative permittivity is 9.8. The substrate thickness is set to be 10 mils, in order to prevent unwanted substrate modes.

The antenna configuration with the aforementioned dimensions is shown in Figure 4-2. As mentioned before, the gain of this type of antenna directly depends on the antenna length. However, this dependency is not linear. After increasing the length sufficiently, the gain remains relatively unchanged with the length increment ([28], [29]). This concept can be observed in Figure 4-3. The maximum gain versus the antenna length curve is plotted in this figure. As can be seen in this plot, the maximum gain has a slight drop at the length of approximately $14\lambda_0$ and beyond this length, the gain remains almost unchanged. However, lengths more than two wavelengths are practically unrealizable because of very small cross section to length aspect ratio. The antenna length is chosen to be 8 mm in this project, in order to have more than 10 dB for the entire structure including the feeding network.

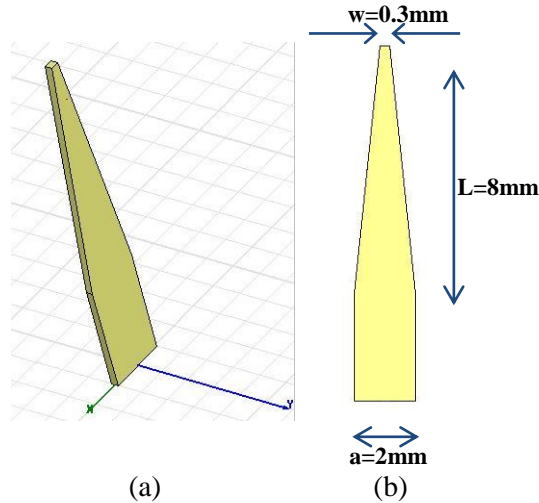


Figure 4-2 Dielectric rod antenna configuration: (a) 3-D view, (b) top view

The corresponding simulation results for radiation pattern and return loss of configuration shown in Figure 4-2 are presented in Figure 4-4 and Figure 4-5 respectively. The return loss shows a wide bandwidth which covers the entire desired frequency range. Dielectric rod antennas are directive and end-fire antennas. The maximum gain which occurs along the axis of the antenna is 12.2 dB.

The other important factor in designing broadband antennas is the antenna gain bandwidth. To ensure the gain coverage for the entire frequency band, the maximum gain versus frequency curve is depicted in Figure 4-6. As illustrated in this figure, the maximum gain variation is less than 1 dB for the frequency range of interest, which is desirable.

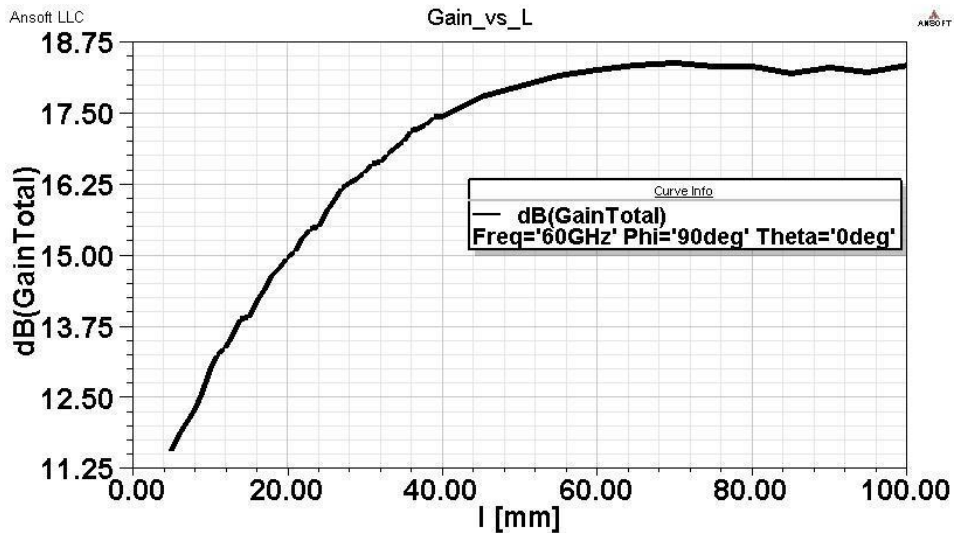


Figure 4-3 Simulated maximum Gain versus length of the antenna

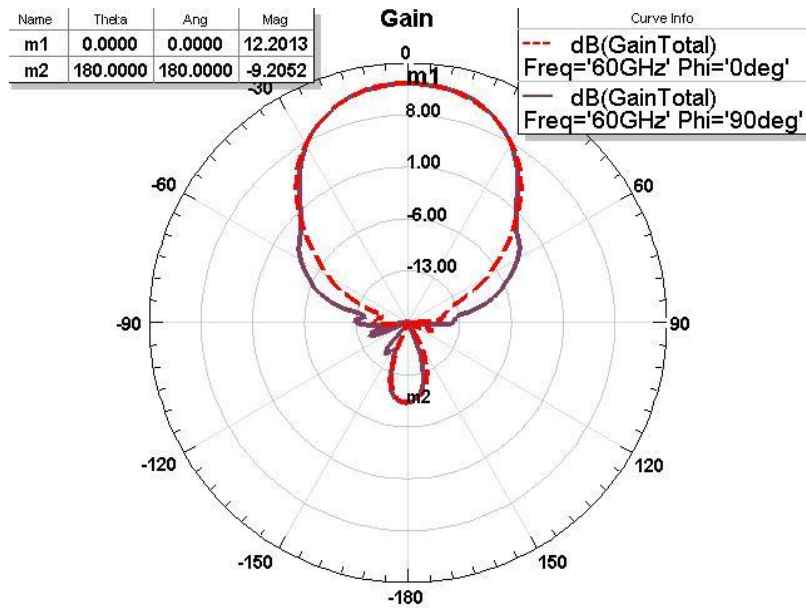


Figure 4-4 Simulation result for E-plane and H-plane pattern of the DW antenna

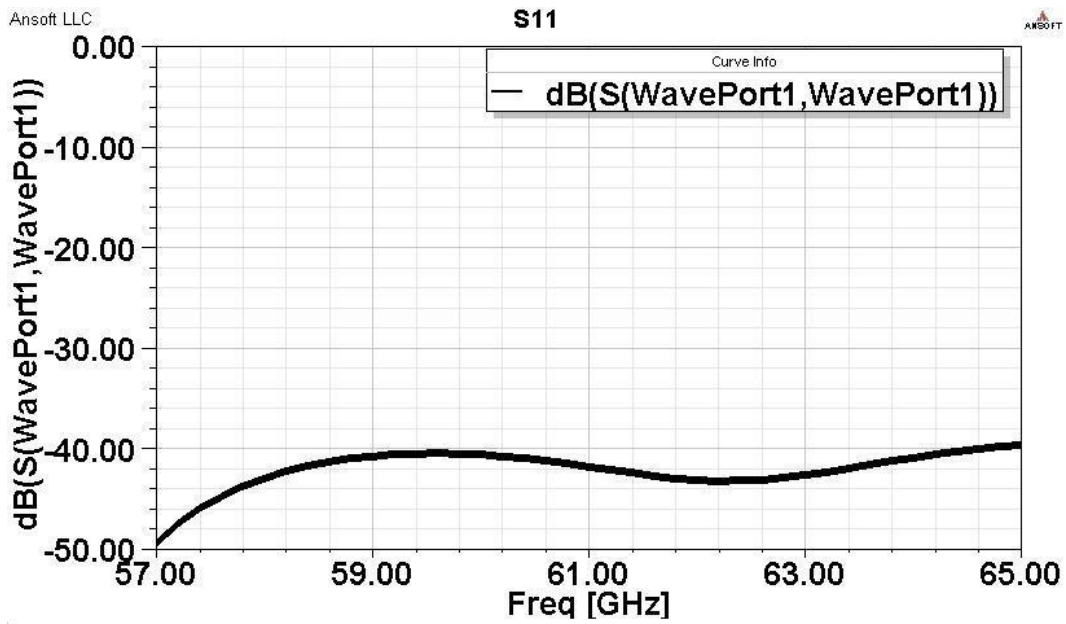


Figure 4-5 Simulated return loss of the DW antenna

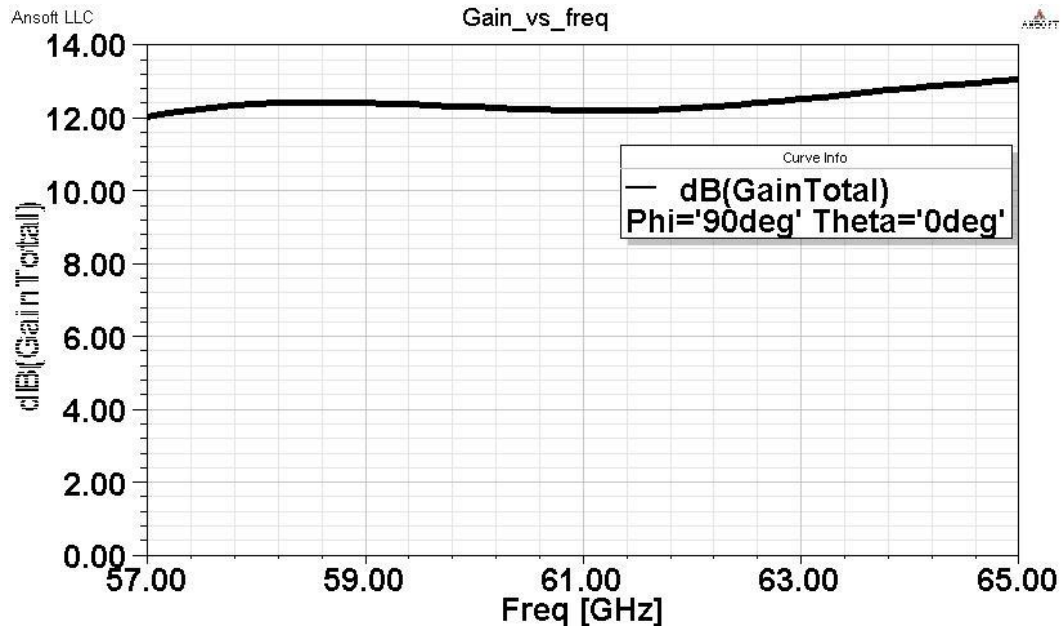


Figure 4-6 Simulated Gain versus frequency for the DW antenna

4.4 Excitation Method for Tapered DW Antenna

In general, dielectric rod antennas can be excited using either the slot lines or the metallic waveguides [26]. However, in most of the proposed designs, metallic waveguides are employed to excite the antenna. In this project, the focus is to introduce a fully planar structure, in order to facilitate the integration with other planar active and passive components. Hence, the first step is to find an appropriate planar transmission line for exciting the antenna.

Considering the fundamental mode field polarization in the antenna, one can find that there is an x-directed electric field with the maximum in the centre of the DW. In order to have the strongest coupling between the feeding line and the antenna, the feeding line should have the same polarization and strength distribution. Slot line, is a planar transmission line which has the same polarity and can be considered as a suitable feed line for the antenna.

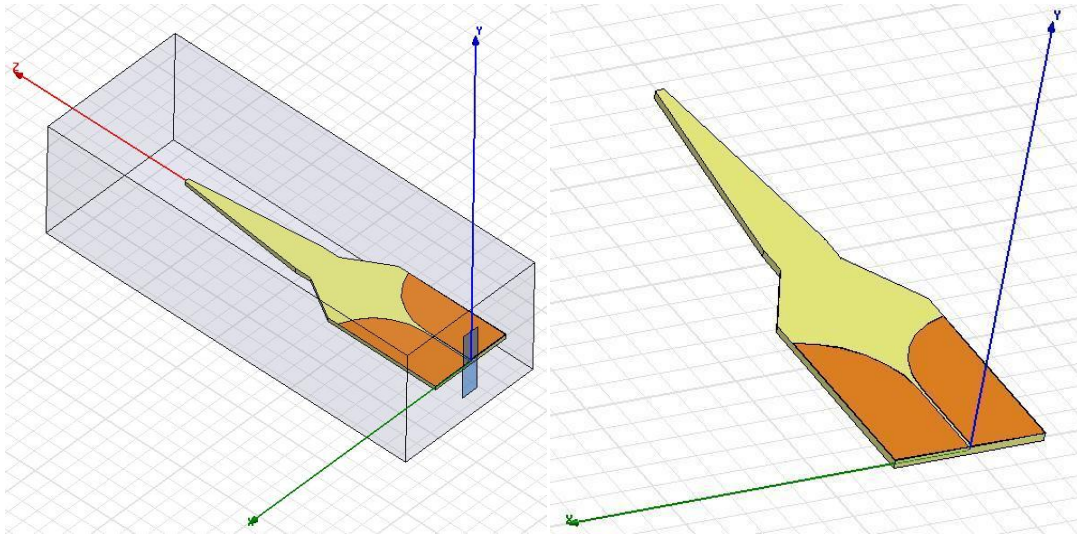
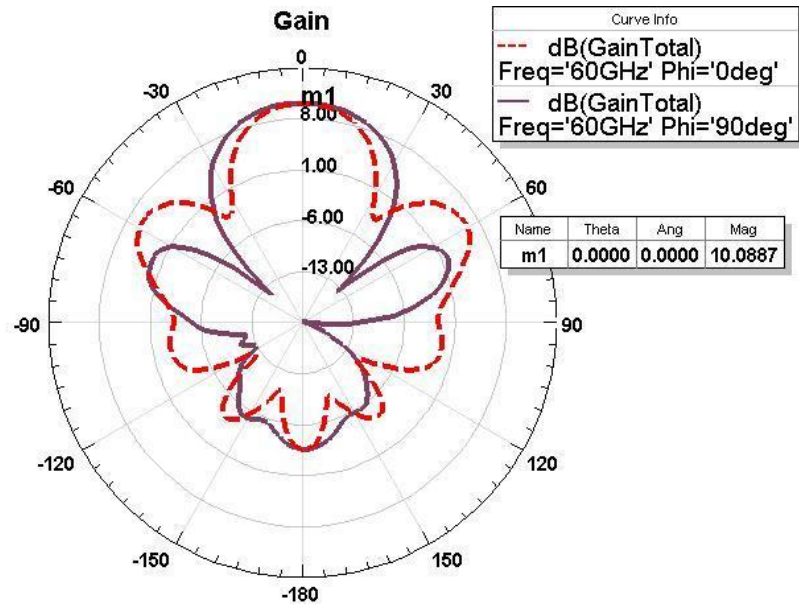


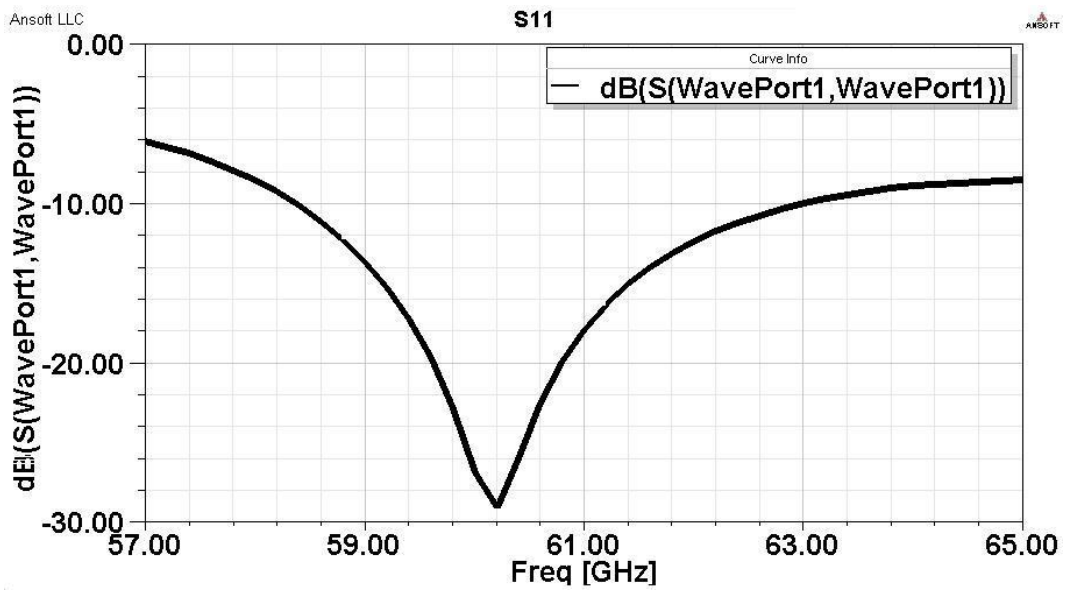
Figure 4-7 DW antenna with slot-line excitation and its corresponding gain pattern

Figure 4-7 shows the antenna with slot line excitation configuration. As can be seen in this figure, the input slot is opened to the lateral sides of the substrate, gradually. This tapered slot can excite the dielectric waveguide properly. The dielectric waveguide is then tapered to connect to the dielectric rod antenna. The simulation results can be observed in Figure 4-8. The wide bandwidth of the return loss curve confirms the desired match between slot line and the antenna.

Although the slot line is appropriate to excite this type of antennas, it is not a common transmission line and thus, a transition between the slot line and one of the conventional transmission lines is required. CPW is chosen in this project since it does not have any ground plane in the bottom side of substrate. In addition, having the ground planes in the same side can be used to flip-chip mounting of MMIC devices prior to the antenna. Design procedure of the CPW-to-slot line transition is explained in the following section.



(a)



(b)

Figure 4-8 Simulation results for DW antenna with slot line excitation: (a) Gain pattern, and (b): S_{11}

4.5 CPW to Slot Line Transition Design

In this section, a literature review is presented on CPW to slot line transitions, followed by the proposed design for CPW to slot line transition in this project.

4.5.1 Literature Review on CPW to Slot Line Transitions

Different types of structures have been proposed for CPW to slot line transition in various frequency ranges. Some examples of the proposed configurations are presented in Figure 4-9. The geometries shown in Figure 4-9(a) are proposed in [30], [31]. Considering the CPW line as two parallel slot lines, one of them is opened at the end and the power is transferred to the slot line by the other arm. The bandwidth of the transition is limited by the bandwidth of the open circuit. In other words, since the circular and rectangular hollow patches provide open circuit conditions with more bandwidth, their final transitions are more wideband. The transitions are designed to operate in the range of 1-4 GHz frequencies. A size reduction has been achieved in the configuration proposed in [32] with the aid of spiral stubs. This transition is illustrated in Figure 4-9(b). The operating frequency for this transition is 2-3 GHz.

All of the aforementioned geometries are proposed to operate at lower microwave frequencies (S and C band). When the desired frequency is increased, such structures cannot be used anymore because of the existence of unwanted radiations. Very broadband prototypes have been reported in [33] and [34] (see Figure 4-9(c)). Although they are operating at higher frequencies up to 25 GHz, they have still the radiation problem when scaling to 60 GHz frequency range. In [35], the concept of slow wave has been exploited to make a delay in one of the CPW arms. The transition geometry is shown in Figure 4-9(d). The transition is operating at 12-16 GHz frequency range. Designing similar transition for 60 GHz frequency results in very thin line widths. Therefore, the structure would be almost unrealizable or very difficult to fabrication at such frequencies. A very broadband prototype is proposed in [36] and [37]. The geometry is depicted in Figure 4-9(e) and the structure is designed to operate at 15 GHz frequency. The transition mechanism is explained as follows.

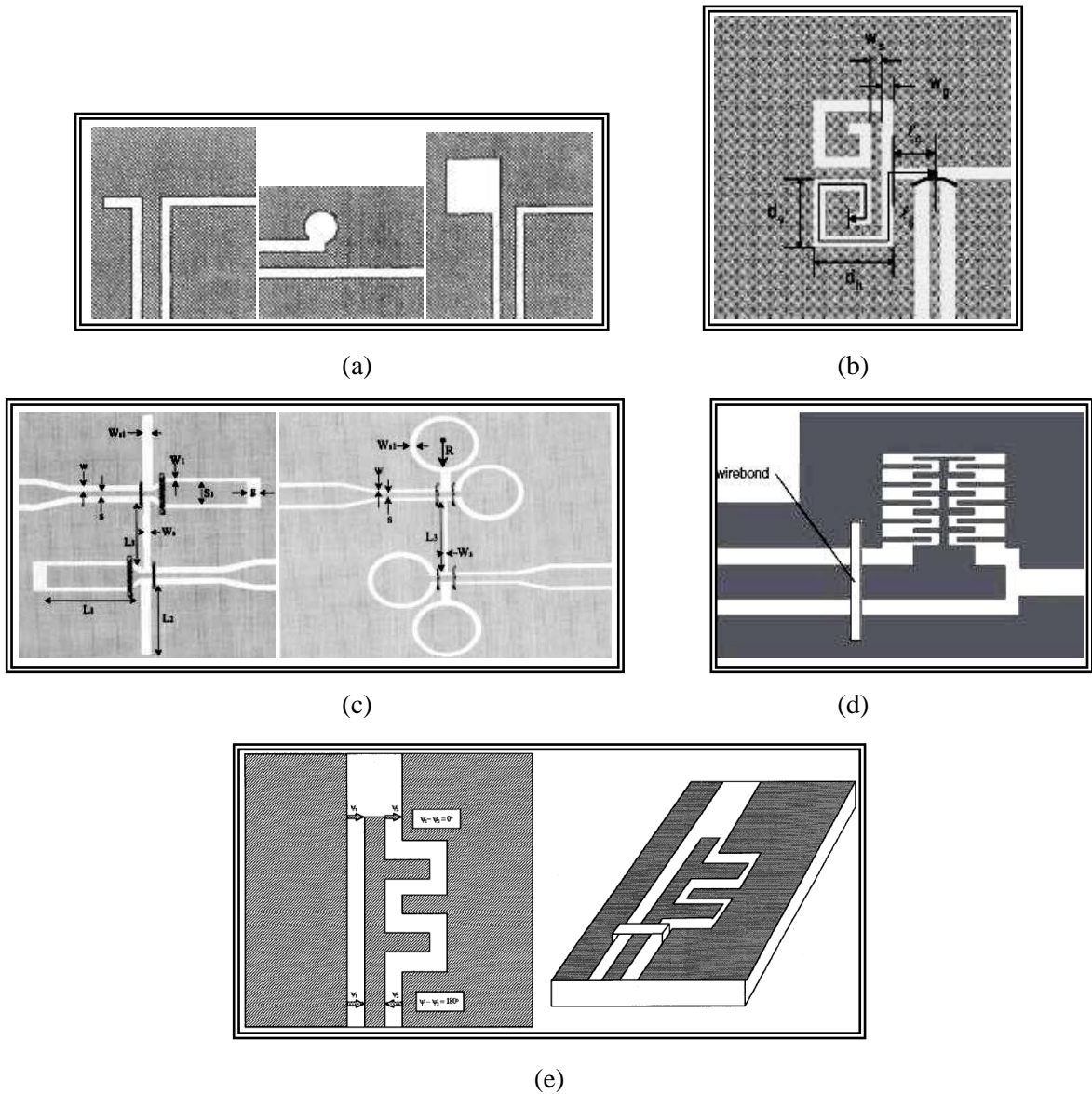


Figure 4-9 CPW-to-Slot line transition configurations: (a) Figure 1 of reference [38], (b) Fig. 1 of reference [32], (c) Fig. 3 and Fig. 9 of reference [34], (d) Fig. 3 of reference [35], and (e) Fig. 1 of reference [36]

Consider the CPW line in Figure 4-9(e) as two parallel slot lines. Based on the CPW field polarization, one can realize that these two slot lines are 180 degrees out of phase. Using either the slow wave (Figure 4-9(d)) or two stubs (Figure 4-9(e)) in one of the slot lines, a 180° phase shift is produced in the corresponding slot line, making both lines in phase at the end of the merging point. By adjusting the stub length in Figure 4-9 (e), the proper delay at certain frequency can be achieved.

After making the slot lines in phase, they are merged to a single slot line. The fields would be adding up constructively at this stage. In this project, the proposed prototype of [37] is employed to design a CPW to slot line transition at 60 GHz frequency. The designed configuration is presented in Figure 4-10. As can be seen in this figure, after merging two slot lines to one, the slot line is tapered to a narrower width in order to have 50 ohms impedance.

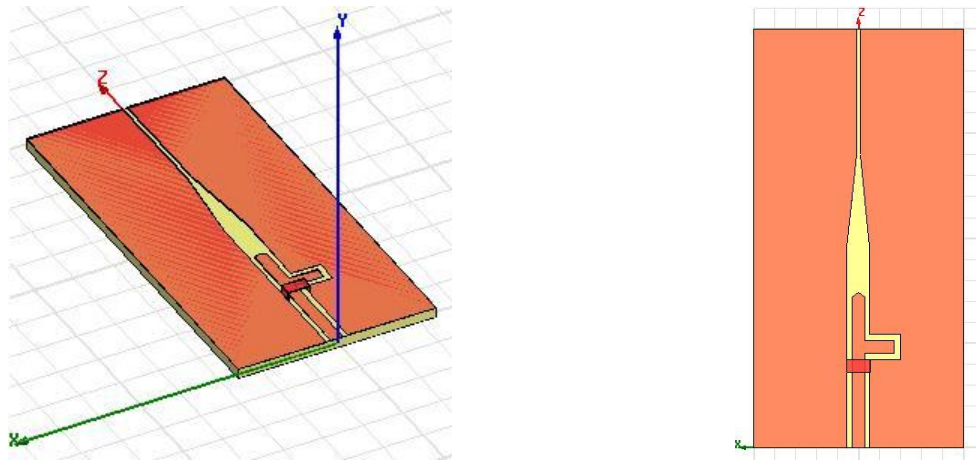


Figure 4-10 CPW-to-Slot line transition for 60 GHz operational frequency

4.5.2 CPW to Slot Line Transition Design

Figure 4-10 shows the final configuration of the designed transition [39]. The x-directed electric field distribution in different positions along the transition has been depicted in Figure 4-11. The plots demonstrate the mechanism described previously. At the first stage, the fields are out of phase, as expected for the conventional CPW line (Ex_Line1 in Figure 4-11). Then, having a stub in one side makes the fields in phase (Ex_Line2 in Figure 4-11). Finally, the fields are added up constructively through the slot line, making an x-directed electric field with maximum in the center (Ex_Line5 in Figure 4-11). Note that an air bridge has been placed just before the stub, to connect the ground planes, preventing any unwanted phase difference and have a reference point.

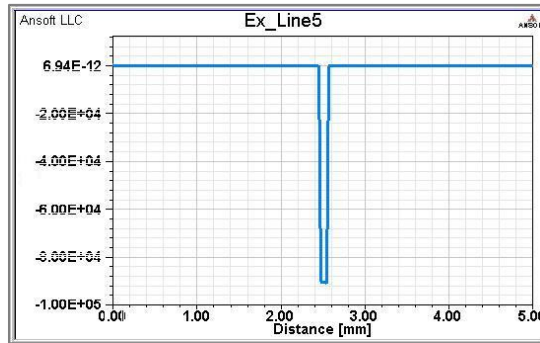
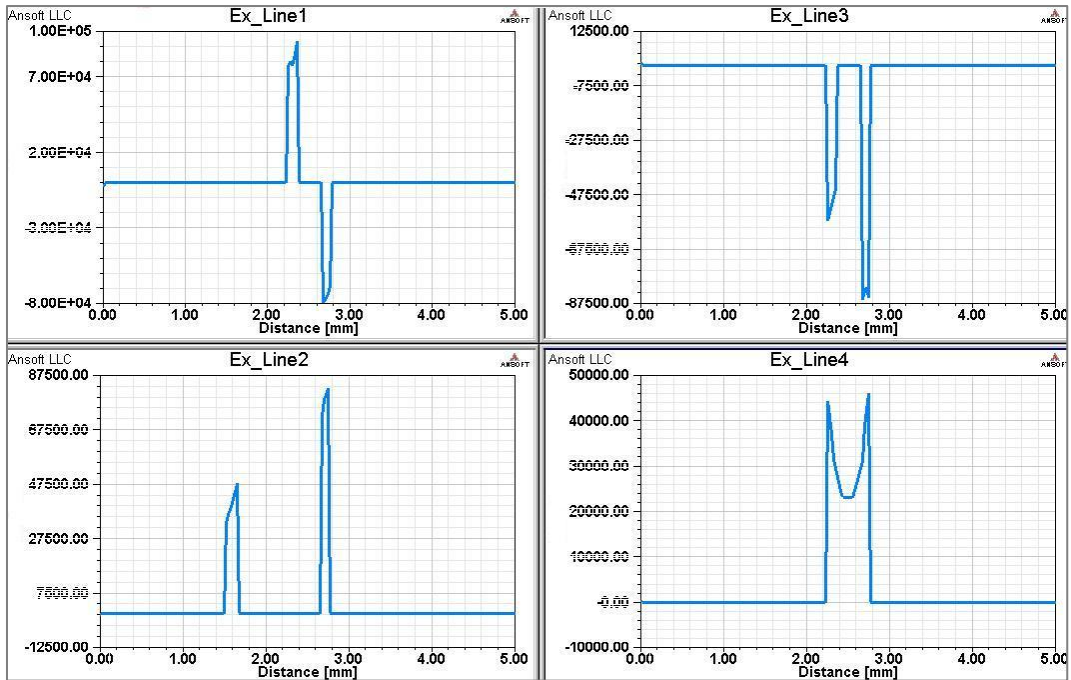
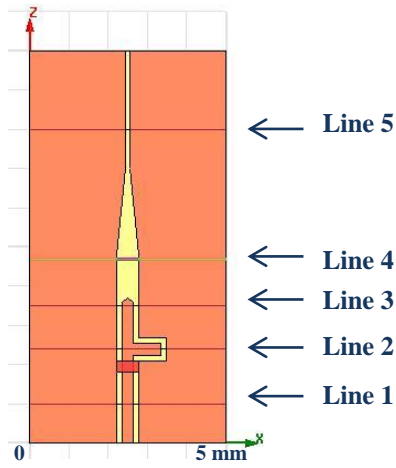


Figure 4-11 Field distribution at the x direction over different cross sections of the transition

S-parameter simulation response of the designed CPW-to-slot line transition is plotted in Figure 4-12. As can be seen in this figure, a well-matched transition has been achieved and the bandwidth covers the entire desired frequency range. Note that at frequencies beyond 64 GHz, the insertion loss is increasing despite of having the return loss better than 30 dB. This is due to the fact that at higher frequencies, the radiation loss will increase.

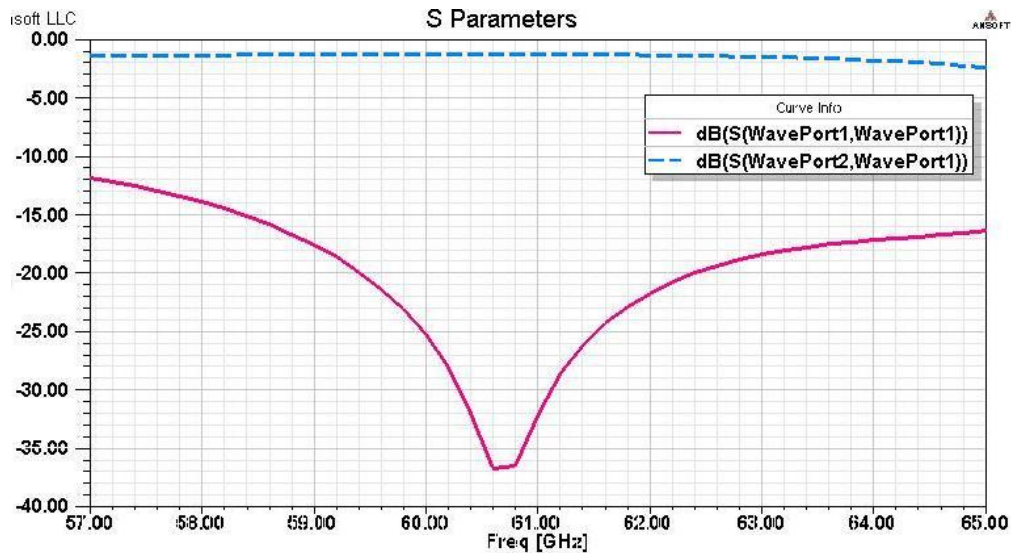


Figure 4-12 Simulated S parameters result of the CPW-to-Slot line transition

4.6 Single Element CPW-fed Tapered DW Antenna

Combining the antenna design in section 4.3 with the CPW to slot line transition design in section 4.5, the entire single element CPW-fed antenna structure has been simulated in HFSS. The configuration is presented in Figure 4-13 and the simulation results are reported in Figure 4-14 and Figure 4-15. The results show 10 dB as the maximum gain in both E-plane and H-plane. The frequency bandwidth covers the entire frequency range of interest (57-64 GHz). The total size of the antenna, including the feeding network, is $5\text{mm} \times 25.5\text{mm}$ which is approximately $\lambda_0 \times 5\lambda_0$.

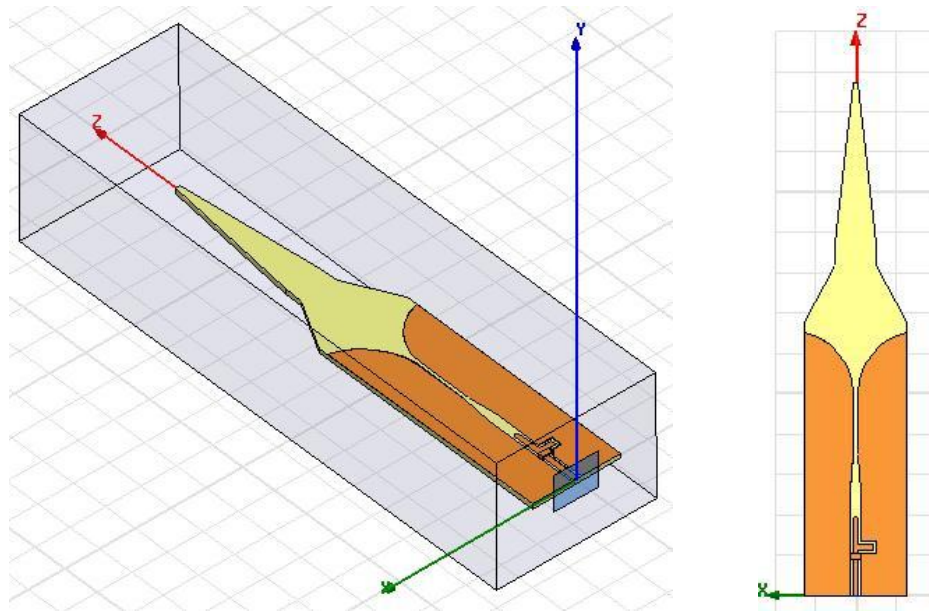


Figure 4-13 Single element antenna configuration

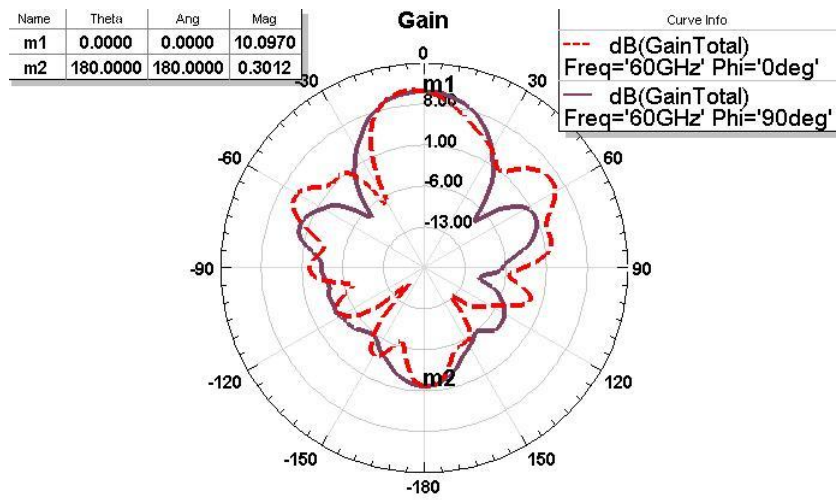


Figure 4-14 E-plane and H-plane gain pattern of the single element antenna

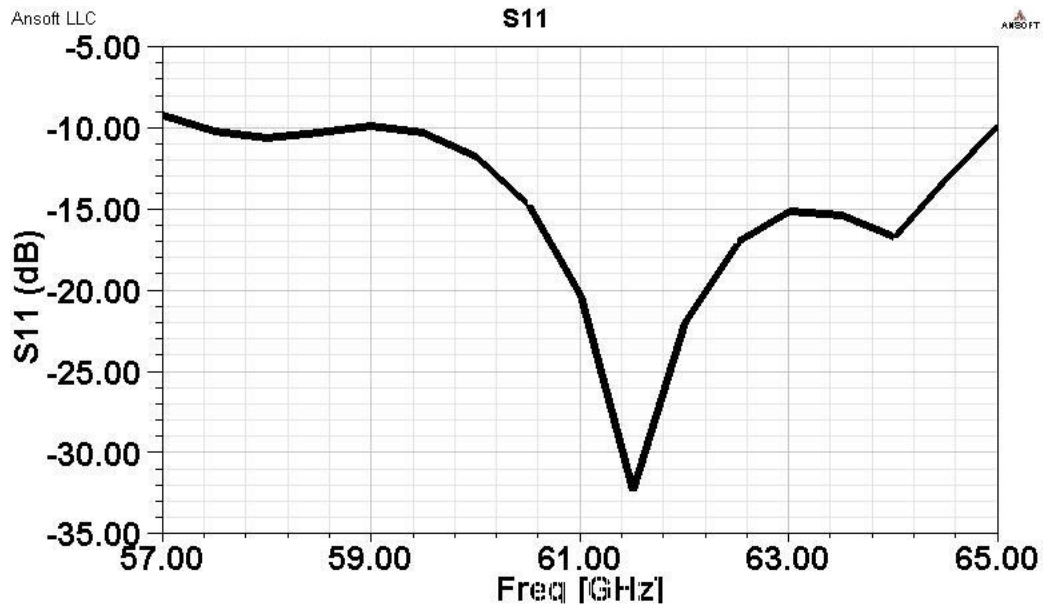


Figure 4-15 Simulated return loss plot for single element antenna

4.7 Curved Tapering of Dielectric Rod Antenna

As mentioned before, there is no exact method for the tapering of dielectric rod antennas [26]. To reduce the total length of the single element antenna, the tapering of DW has been modified to an exponential shape. Figure 4-16 shows this configuration. The advantage of this new tapering is size reduction of about 3 mm as well as preventing sharp corners which is difficult to realize from practical point of view. The simulation results of this structure are plotted in Figure 4-17 and Figure 4-18. As can be observed in the plots, the results are almost similar to the previous design, while ease of fabrication and size reduction has been achieved.

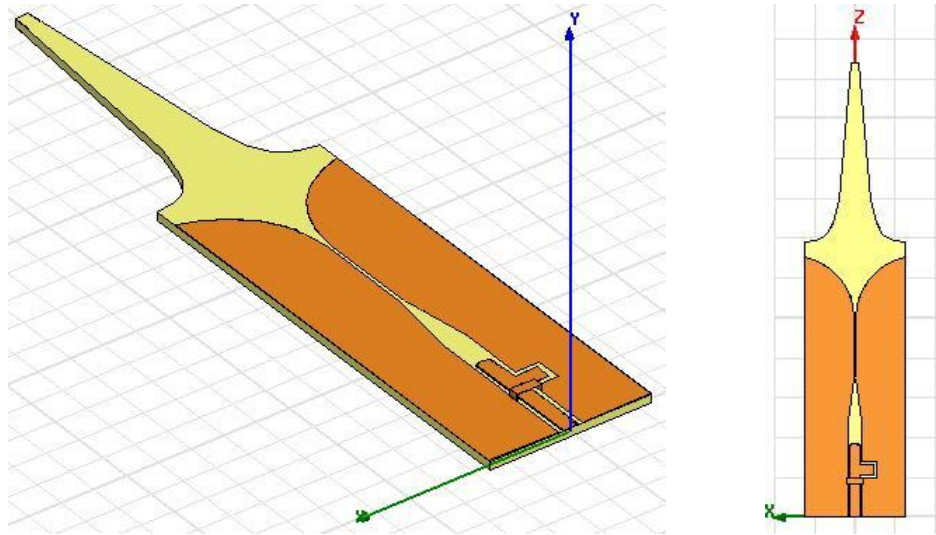


Figure 4-16 Single element antenna with exponential tapering

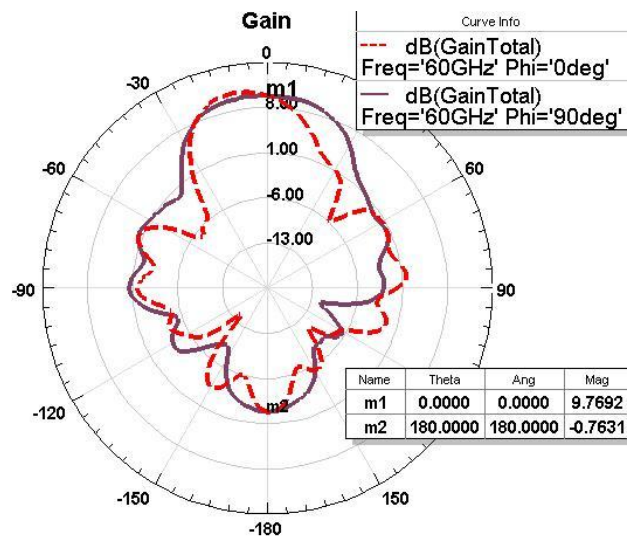


Figure 4-17 Simulation result of gain for the antenna with exponential tapering

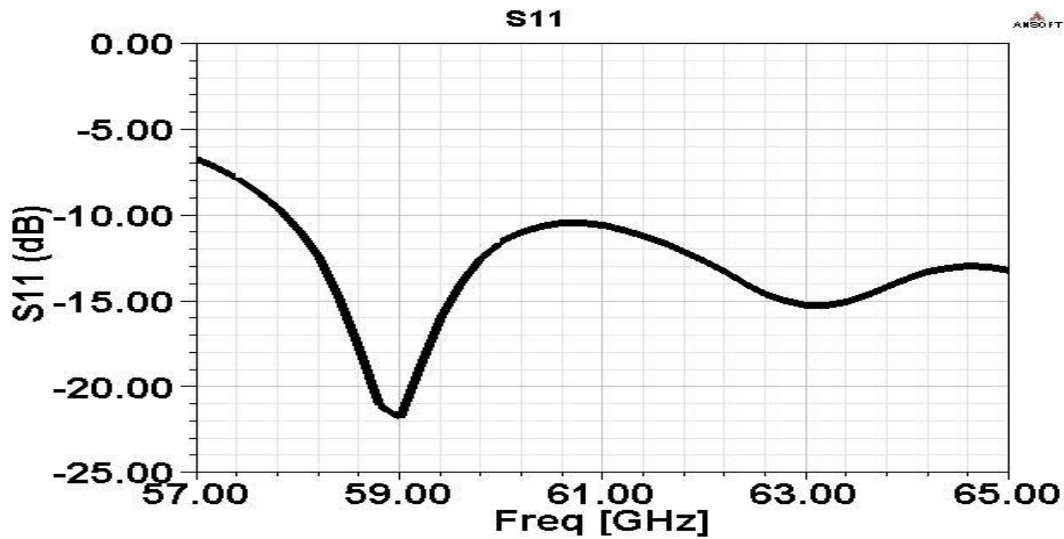


Figure 4-18 Return loss simulation result for antenna with exponential tapering

4.8 Linear Array of Two Elements Antenna

Antenna arrays have many applications in communication systems. Exploiting antennas in array forms improve the total gain significantly. More importantly, combining the antennas with phase shifters facilitate beam steering and beam forming electrically, which has many applications in radar systems, etc. Consequently, the antenna prototype presented in the previous section could be combined with phase shifters in a passive phased array system. To verify the functionality of the antenna in linear array form, a two element array has been designed and the simulation results are presented in this section. The antenna elements have 6 mm centre to centre distance which is $1.2 \lambda_0$ at 60 GHz frequency. The structure is shown in Figure 4-19. As can be seen in this figure, a simple 2-to-1 divider is used to feed the array. The total gain improvement in compare with single element is less than 3 dB, which is theoretically expected. This difference is mainly because of the insertion loss of the divider (about 0.8 dB) and the presence of coupling between two elements. Simulation results of the gain pattern and return loss are plotted in Figure 4-20 and Figure 4-21 respectively.

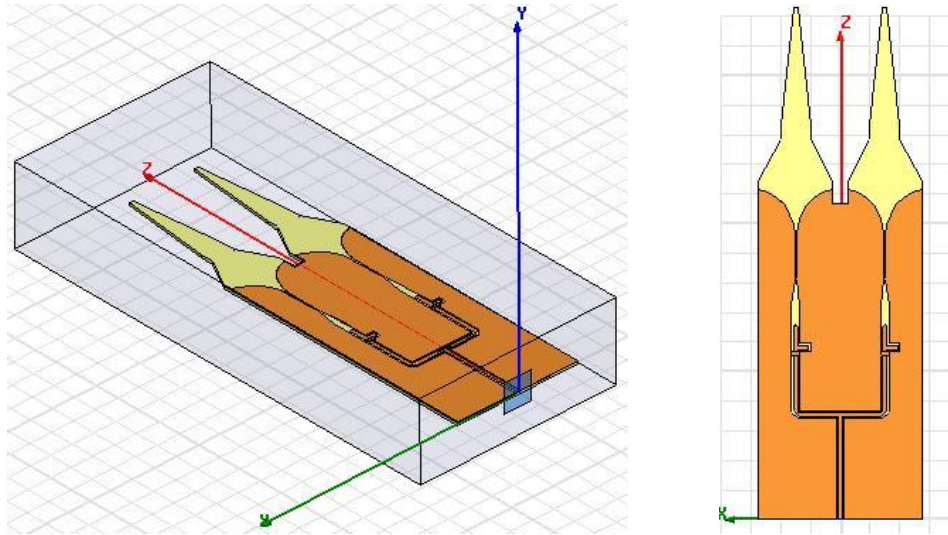


Figure 4-19 Linear array of two elements antenna configuration

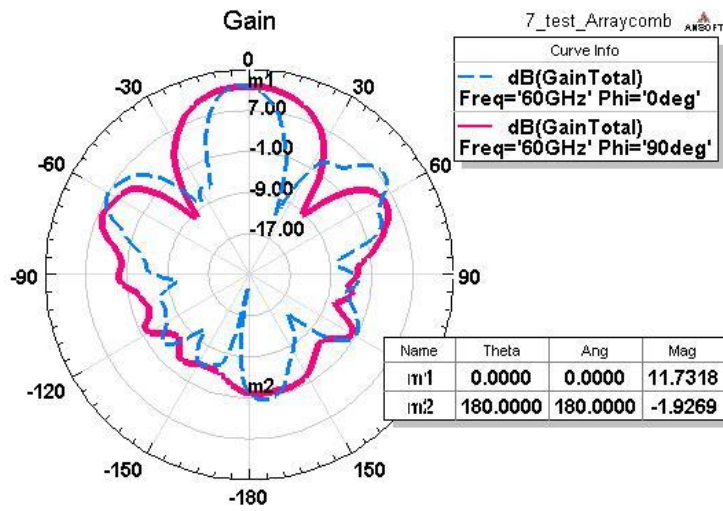


Figure 4-20 Simulation result of the gain pattern for the array antenna

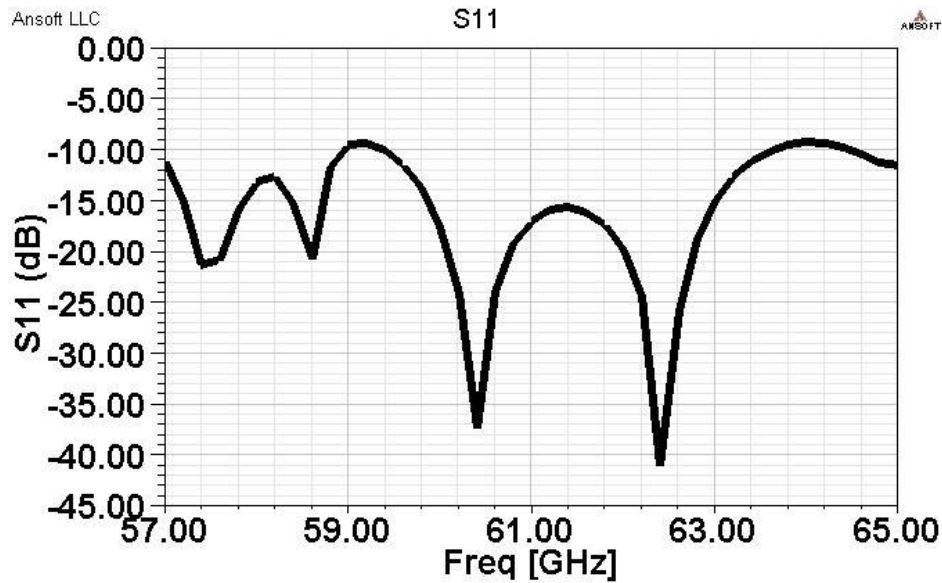


Figure 4-21 Simulation result of the return loss for the array antenna

The CPW input line of the antenna elements make it possible to easily flip-chip MMIC amplifiers and enhance the system performance.

4.9 Fabrication Process

Different techniques can be used to cut the alumina substrate in order to form the proposed tapered antenna shape. The most common available cutting techniques are laser cutting and Waterjet cutting [40]. Waterjet cutting has attracted significant attention because of its unique advantages over the laser cutting. In laser cutting technique, a light beam of 10.6 μm is used to cut the material. Therefore, the process temperature is high and it might change the material properties such as permittivity. In addition, burning at the cutting edges occurs when using this technique due to the high temperature. On the other hand, a jet of pressurized water is used in Waterjet technique to cut the material. This is a cold process and therefore, it has no effect on material properties and the cutting edges are cleaner than laser technique. A full comparison between two techniques can be found in [41].

Several designs have been developed and submitted for fabrication. As presented in previous sections, the total size of the proposed antenna is $5\text{mm} \times 25.5\text{mm}$. Therefore, the configuration has a relatively high length to width ratio. In addition, the substrate thickness is quite thin (10 mil) which makes it very fragile. Therefore, achieving high precision in the tip region of the antenna seems to be a challenging task which is being dealt with in the next phase of the research.

4.10 Summary

Design of a CPW-fed dielectric rod antenna was presented in this chapter. Alumina substrate with the thickness of 10 mils was used for this purpose. The total antenna dimensions, including the feeding network, are 5 mm × 25.5 mm. More than 10 dB gain was shown in the simulation results at 60 GHz frequency and the design was well matched over the desired frequency range (57-64 GHz). In addition, a two element array of the antenna was presented to demonstrate the antenna applications for beam forming and phased-array systems.

Chapter 5

Antenna Design on High Resistive Silicon Substrate

5.1 Introduction

Silicon-based technologies are under focus attention in mm-wave integrated circuit designs due to their very low loss and availability of wide range of low cost and high precision commercial foundries. The high permittivity of about 11.9 for silicon wafers leads to small size designs. In addition, due to the special material properties of silicon, it can be easily and accurately etched to obtain various configurations. An additional advantage for high resistive silicon wafer is its very low loss at high frequencies. Silicon wafers have been developed recently with resistivity of as high as 100 ohm-meter. On the other hand, existence of numerous silicon-based MEMS components has created a unique opportunity for novel antenna structures integrated with control devices.

In the next section, the mechanical support requirement for tapered dielectric rod antenna on high resistive silicon is explained. Design of the CPW to slot line transition is presented in section 5.3. Simulation results of the proposed single element antenna are reported in 5.4.

5.2 Mechanical Support Requirement

As mentioned in previous chapters, the substrate thickness has significant effects on the antenna design performance. The thickness of the substrate was chosen to be 10 mil in previous chapter since experiments show that thicker substrates deteriorate the antenna performance significantly. Therefore, due to the fragility of a 10 mil substrate, mechanical supports should be designed to protect the entire design. Utilizing silicon machining and etching capabilities, a new design is presented in the next section to ensure the mechanical stability of the design.

The proposed design uses a thick substrate which is etched underneath the radiating region. A sample design presented in this chapter consists of the antenna with thickness of 10 mil in radiating regions with robust mechanical supports of 20 mil thickness. The proposed antenna design in this chapter follows the same procedure presented in previous chapter.

5.3 Design of the CPW to Slot Line Transition on High Resistive Silicon

Figure 5-1 shows the proposed configuration for the CPW-to-Slot line transition. As can be seen in layer configuration (Figure 5-2), two layers of high-resistive silicon material (layers 2 and 4) are

bonded with a thin layer of silicon oxide (layer 3). The metal layer (which is 2 micron gold) is placed on the top silicon layer. The bottom silicon layer will be etched underneath the transition, leaving the transition on a 10 mil thickness substrate.

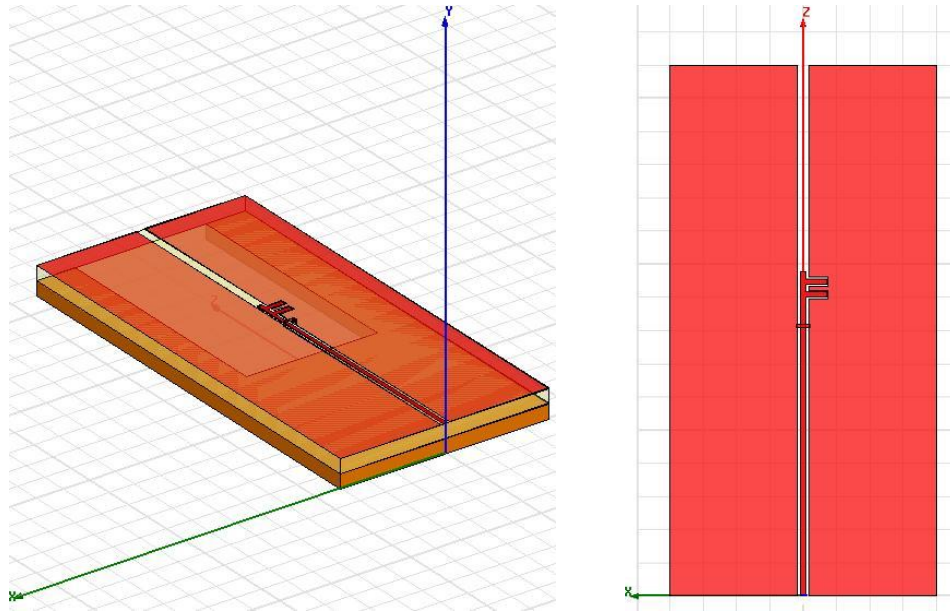


Figure 5-1 CPW to slot line transition on high resistive silicon substrate

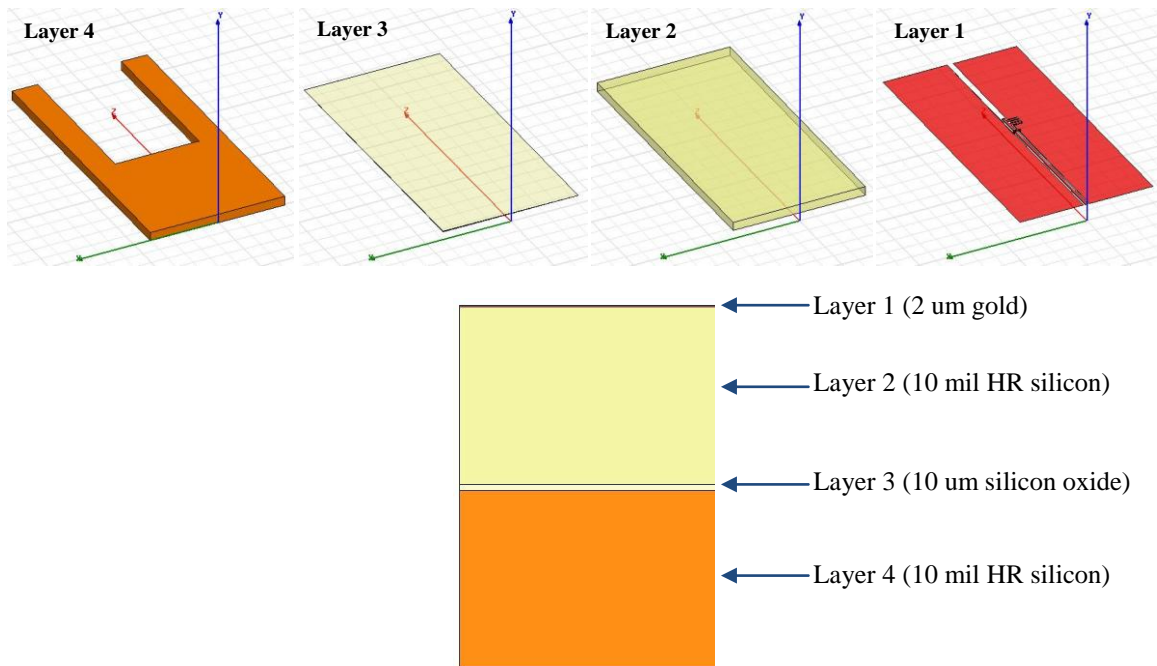


Figure 5-2 Layer configuration of the CPW to slot line transition

The proposed structure has been simulated in HFSS and the S parameter plots are shown in Figure 5-3. The results indicate a well matched bandwidth over 57-70 GHz and the insertion loss is less than 1.5 dB over the entire frequency band.

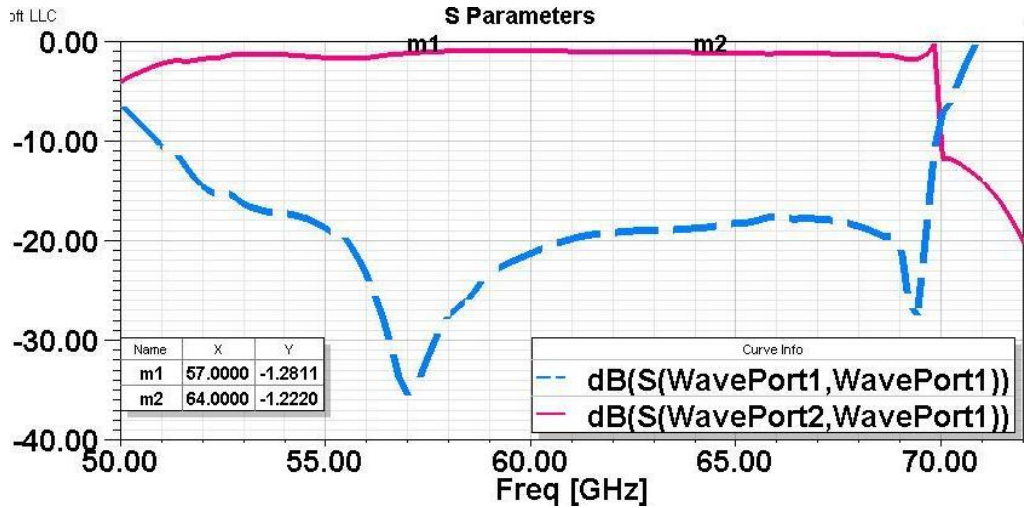


Figure 5-3 Simulation results of S parameters for the CPW to slot line transition on HR⁴ silicon

5.4 Single Element Tapered Dielectric Antenna on High Resistive Silicon

The design of the antenna has been done by one of the members of our research group, Saman Jafarloo. The tapering shape and the total antenna length have been optimized by him. The antenna design is then connected to the transition to form the final CPW-fed single element antenna. The final structure is shown in Figure 5-4. Two silicon anchors on the top layer are mechanical supports for the antenna and protect it from breaking in the fabrication process. Simulation results for this structure show 9.8 dB gain, with bandwidth of more than 16%. It should be mentioned that the (simulated) efficiency of this structure is more than 90% due to exploiting a very low loss dielectric material and having no conductor in the antenna structure.

⁴ High Resistive

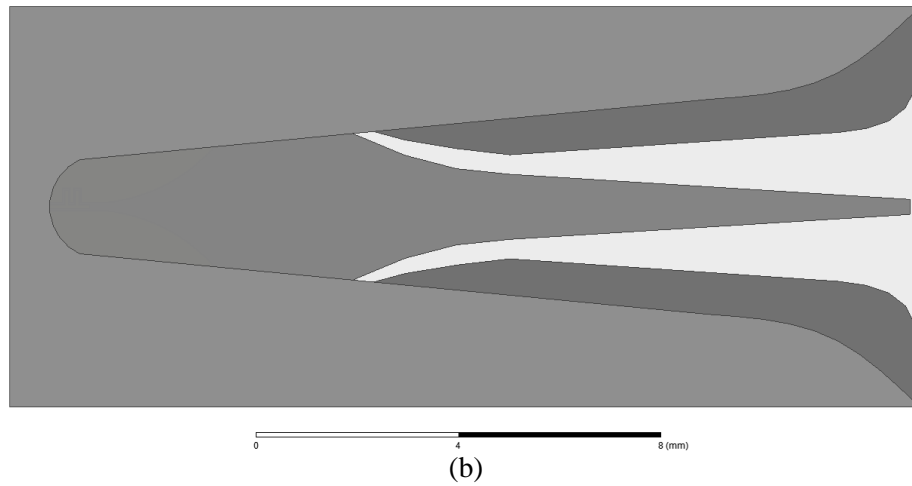
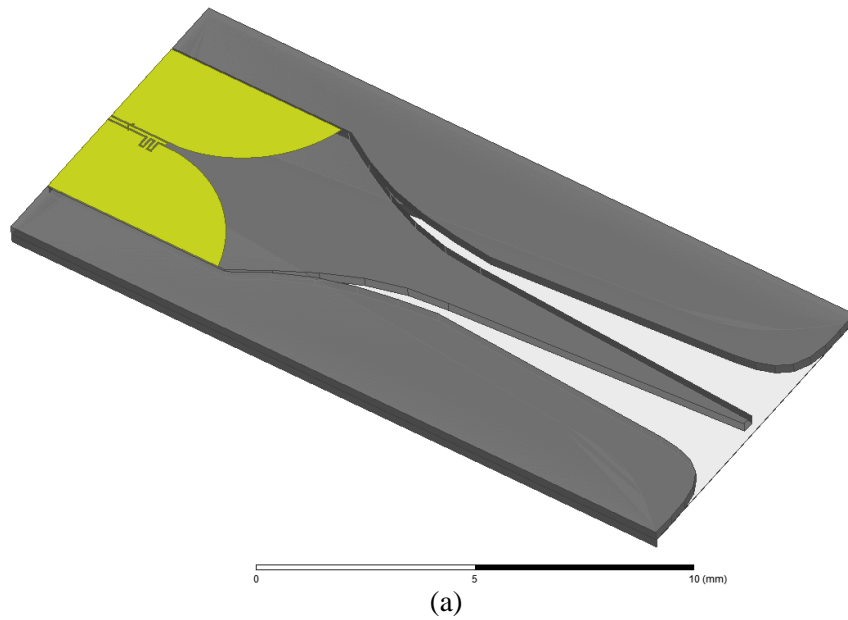


Figure 5-4 Single element antenna on high-resistive silicon: (a) 3D view, and (b) bottom view

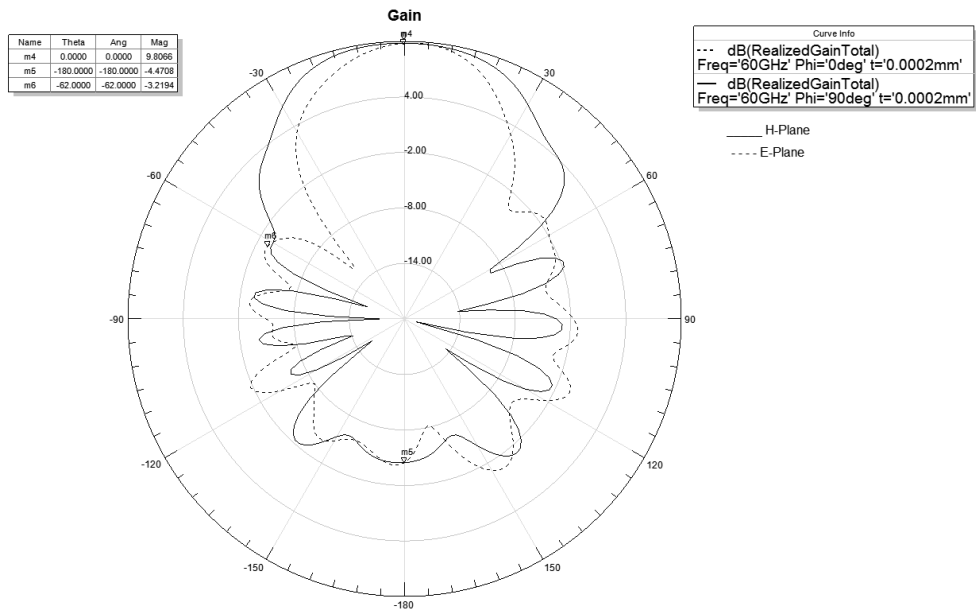


Figure 5-5 Simulation result of gain for the single element antenna on high- resistive silicon

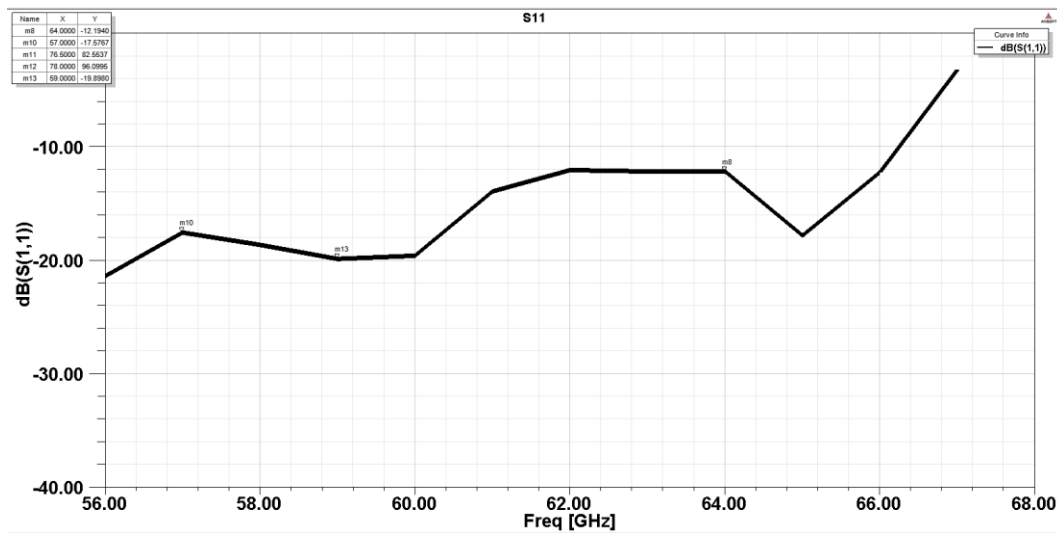


Figure 5-6 Return loss simulation result for single element antenna on high-resistive silicon

Chapter 6

Conclusion and Future Work

6.1 Conclusion

Design of a planar tapered dielectric rod antenna was presented in this project. The design was presented on two common low loss substrates: alumina and high resistive silicon. The fully planar structure and CPW input make the antenna compatible with other components in communication front-ends. In addition, the antenna has more than 90% (simulated) efficiency due to the dielectric nature of the structure. The antenna is high gain and wide bandwidth, which make it a good candidate for short range wireless applications. The conductors are needed only on top side, preventing any difficulties in back metallization. Since the antenna structure is dielectric based, it can be easily scaled to higher operating frequencies. A linear array of two elements for the designed antenna was designed and the simulation results were presented to show the antenna capability in phased array applications.

6.2 Future Work

Future work for this project can be summarized as follows:

- Optimization and shrinking the size of the antenna.
- Dealing with fabrication challenges of antenna design on alumina substrate.
- Measuring the fabricated configurations and compare the experimental results with the simulation results.
- Integrate the antenna array with phase shifters to form a passive phased array system

Bibliography

- [1] Shao-Qiu Xiao, Ming-Tuo Zhou, and Yan Zhang, *Millimeter wave technology in wireless Pan, Lan, and Man.*: Auerbach Publications, Taylor & Francis Group, 2008.
- [2] Rudy M. Emrick, "On-Chip Antenna Element and Array Design for Short Range Millimeter-Wave Communications," Ohio State University, PhD Thesis 2007.
- [3] Mohammad Fakharzadeh, Mohammad-Reza Nezhad-Ahmadi, Behzad Biglarbegan, Javad Ahmadi-Shokouh, and Safieddin Safavi-Naeini, "CMOS Phased Array Transceiver Technology for 60 GHz Wireless Applications," *IEEE Transactions on Antennas and Propagation*, vol. 58, no. 4, pp. 1093-1104, April 2010.
- [4] <http://www.ieee802.org/15/pub/TG3c.html>.
- [5] <http://www.WirelessHD.org>.
- [6] <http://www.wigwam-project.com>.
- [7] Behzad Biglarbegan, Mohammad Fakharzadeh, Dan Busuioc, Mohammad-Reza Nezhad-Ahmadi, and Safieddin Safavi-Naeini, "Optimized Microstrip Antenna Arrays for Emerging Millimeter-Wave Wireless Applications," *IEEE Transactions on Antennas and Propagation* , vol. 59, no. 5, pp. 1742-1747, May 2011.
- [8] Keren Li, Tomoaki Sato, and Naoki Kajitani, "Wideband Planar Antennas for Millimeter-wave Wireless Communications," in *Antennas and Propagation Society International Symposium*, 2008, pp. 1-4.
- [9] Mahmoud Al Henawy and Martin Schneider, "Planar Antenna Arrays at 60 GHz Realized on a New Thermoplastic Polymer Substrate," in *European Conference on Antennas and Propagation (EuCAP)*, 2010, pp. 1-5.
- [10] Sergey Dudorov, Mikko Kyrö, Cyril Luxey, Clemens Icheln, Robert Staraj, and Pertti Vainikainen Sylvain Ranvier, "Low-Cost Planar Omnidirectional Antenna for mm-Wave Applications," *Antennas and Wireless Propagation Letters*, vol. 7, pp. 521-523, 2008.
- [11] Ramadan A. Alhalabi and Gabriel M. Rebeiz, "High-Gain Yagi-Uda Antennas for Millimeter-Wave Switched-Beam Systems," *IEEE Transactions on Antennas and Propagation*, vol. 57, no. 11, pp. 3672-3676, November 2009.
- [12] Ramadan A. Alhalabi, Yi-Chyun Chiou, and Gabriel M. Rebeiz, "Self-Shielded High-Efficiency Yagi-Uda Antennas for 60 GHz Communications," *IEEE Transactions on Antennas and*

Propagation, vol. 59, no. 3, pp. 742-750, March 2011.

- [13] Trevor Bird, and Benjamin Johnston Stephen Hanham, "A Ring Slot Excited Dielectric Rod Antenna for Terahertz Imaging," in *Antennas and Propagation Society International Symposium*, 2007, pp. 5539-5542.
- [14] A. Y. Simba, M. Yamamoto, T. Nojima, and K. Itoh, "Linear array of image NRD guide-based dielectric rod antenna fed by slotted rectangular waveguide," *Microwave, Antennas and Propagations*, vol. 152, no. 5, pp. 331-336, October 2005.
- [15] Andreas Patrovsky and Ke Wu, "94-GHz Planar Dielectric Rod Antenna With Substrate Integrated Image Guide (SIIG) Feeding," *IEEE Antennas and Wireless Propagation Letters*, vol. 5, pp. 435-437, 2006.
- [16] A. Patrovsky and K. Wu, "Active 60 GHz front-end with integrated dielectric antenna," *Electronics Letters*, vol. 45, no. 15, July 2009.
- [17] A. Patrovsky and Ke Wu, "94-GHz Broadband Transition from Coplanar Waveguide to Substrate Integrated Image Guide (SIIG)," in *International Microwave Symposium (MTT-S)*, 2007, pp. 1551-1554.
- [18] J. E. GOELL, "A Circular-Harmonic Computer Analysis of Rectangular Dielectric Waveguides," *The Bell System Technical Journal*, pp. 2133-2160, September 1969.
- [19] Kenneth L. Klohn, Robert E. Horn, Harold Jacobs, and Elmer Freibergs, "Silicon Waveguide Frequency Scanning Linear Array Antenna," *IEEE Transactions on Microwave Theory and Techniques*, vol. MTT-26, no. 10, pp. 764-773, October 1978.
- [20] E. A. J. Marcatali, "Dielectric Rectangular Waveguide and Directional Coupler for Integrated Optics," *The Bell System Technical Journal*, pp. 2071-2102, 1969.
- [21] Gabriel M. Rebeiz, "Millimeter-Wave and Terahertz Integrated Circuit Antennas," *Proceedings of the IEEE*, vol. 80, no. 11, pp. 1748-1770, 1992.
- [22] Satoshi Kobayashi, Raj Mittra, and Ross Lampe, "Dielectric Tapered Rod Antennas for Millimeter-Wave Applications," *IEEE Transactions on Antenna and Propagation*, vol. AP-30, no. 1, pp. 54-58, January 1982.
- [23] Junji Yamauchi, and Hisamatsu Nakano Takashi Ando, "Numerical Analysis of a Dielectric Rod Antenna—Demonstration of the Discontinuity-Radiation Concept," *IEEE Transactions on Antennas and Propagation*, vol. 51, no. 8, pp. 2007-2013, August 2003.

- [24] J. R. James, "Engineering approach to the design of tapered dielectric-rod and horn antennas," *Radio and Electronic Engineer*, vol. 42, no. 6, pp. 251-259, June 1972.
- [25] F. J. Zucker, "Surface and leaky-wave antennas," in *antenna engineering handbook.*: New York: McGraw-Hill, 1961.
- [26] Jilrgen Richtecr and Lorenz-Peter Schmidt, "Dielectric Rod Antennas as Optimized Feed Elements for Focal Plane Arrays," in *Antennas and Propagation Society International Symposium*, 2005, pp. 667-670.
- [27] Qiu Jing-hui and Wang Nan-nan, "Optimized Dielectric Rod Antenna for Millimeter Wave FPA Imaging System," in *International Workshop on Imaging Systems and Techniques (IST 2009)*, Shenzhen,China, 2009, pp. 147-150.
- [28] Yih Shiau, "Dielectric Rod Antennas for Millimeter-Wave Integrated Circuits," *IEEE Transactions on Microwave Theory and Techniques*, pp. 869-872, November 1976.
- [29] Pramendra Kumar Verma, Raj Kumar, and Mahakar Singh, "Design and Simulation of Dielectric Tapered Rod as Feed for Dielectric Lens Antenna at 140 GHz," in *International Conference on Microwave - 08*, 2008, pp. 233-235.
- [30] Think Q. Ho and Stephen M. Hart, "A Broad-Band Coplanar Waveguide To Slotline Transition," *IEEE Microwave and Guided Wave Letters*, vol. 2, no. 10, pp. 415-416, October 1992.
- [31] C. H. Ho, L. Fan, and K. Chang, "Experimental investigations of CPW-slotline transitions for uniplanar microwave integrated circuits," in *Microwave Symposium Digest*, vol. 2, 1993, pp. 877-880.
- [32] Yo-Shen Lin and Chun Hsiung Chen, "Design and Modeling of Twin-Spiral Coplanar-Waveguide-to-Slotline Transitions," *IEEE Transactions on Microwave Theory and Techniques*, vol. 48, no. 3, pp. 463-466, March 2000.
- [33] K. Hettak et al., "Improved CPW to slotline transitions," in *Microwave Symposium Digest*, vol. 3, 1996, pp. 1831-1834.
- [34] Khelifa Hettak et al., "New Miniature Broad-Band CPW-to-Slotline Transitions," *IEEE Transactions on Microwave Theory and Techniques*, vol. 48, no. 1, pp. 138-146, January 2000.
- [35] J. Naylor, T. Weller, M. Smith, and J. Culver, "Slow-wave CPW slot-line transition," *Microwaves, Antennas, and Propagation*, vol. 152, no. 5, pp. 297-298, October 2005.
- [36] Kuang-Ping Ma and Tatsuo Itoh, "A new broadband Coplanar Wavwguide to slotline transition,"

IEEE MTT-S DIGEST, pp. 1627-1630, 1997.

- [37] Kuang-Ping Ma, Yongxi Qian, and Tatsuo Itoh, "Analysis and Applications of a New CPW–Slotline Transition," *IEEE Transactions on Microwave Theory and Techniques*, vol. 47, no. 4, pp. 426-432, April 1999.
- [38] F. Alessandri, W. Menzel, M. Mongiardo, and R. Somntin, "Efficient full-wave analysis of coplanar waveguide to slotline interconnections with finite metallization thickness accounting for air bridge effects," in *Microwave Symposium Digest*, vol. 2, 1994, pp. 875-878.
- [39] Z. Sotoodeh, B. Biglarbegian, M. R. Nezhad-Ahmadi, M. Fakharzadeh, and S. Safavi-Naeini, "A Wideband and High Gain Antenna for Short-range mm-wave Wireless Applications," in *Antennas and Propagation Society International Symposium (APSURSI)*, 2010, pp. 1-4.
- [40] <http://www.waterjetcutting.ca/wVc/index.asp>.
- [41] http://www.teskolaser.com/waterjet_cutting.html.